Investigating Processes of Glacial Erosion and Cirque Formation by Numerical Modeling and Field Observations in the Southern Sierra Nevada, California

Sabrina Marie Belknap

A thesis submitted to the faculty of the University of North Carolina at Chapel Hill in partial fulfillment of the requirements for the degree of Master of Science in the Department of Geological Sciences (Geomorphology).

Chapel Hill
2009

Approved by:

Michael Oskin

Jonathan Lees

Donna Surge

ABSTRACT

Sabrina Marie Belknap

Investigating Processes of Glacial Erosion and Cirque Formation by Numerical Modeling and Field Observations in the Southern Sierra Nevada, California

(Under the direction of Michael Oskin)

Existing rules for erosion by glaciers are inconsistent with observations of significant cirque retreat. To better understand the processes of cirque formation and expansion, two separate studies were commenced: a field study and a numerical model. These studies were designed to test the hypothesis that cirques ultimately form from fluctuating levels of glacial occupation. Morphometric characteristics of four cirques indicate that cirque expansion may result from growth of a riegel from bedrock shoulders. Variable ice flow directions determined from striae data in three of the cirques correlate with areas of greater ice thickness. Numerical modeling efforts show that overdeepenings may form from ice flow through existing constrictions, but only when a threshold quarrying rule is used. They also highlight the importance of the relative efficacy of abrasion and quarrying when modeling and indicate that quarrying is a more efficient process than abrasion.

Table of Contents

List of Figures

Figure

Introduction

Late Cenozoic global cooling and commensurate increase in glaciation is likely to have had a profound impact on erosion rates and relief structure in mountain belts worldwide. Compared to other instruments of erosion, glaciers are very rapid erosive agents, demonstrating as much as ten times the erosion rate of rivers (Hallet et al., 1996). This efficient removal of material from high elevations by glacial bedrock erosion can cause isostatic uplift of peaks, disrupting weather patterns with consequent effects on global climate (Molnar and England, 1990). Moreover, because glaciers are a dominant factor in eroding many mountain ranges, an increase in alpine glaciation enhances overall erosion rates. Glacial abrasion of bedrock, plucking and quarrying of rock fragments, and frost wedging are all processes that expose a greater surface area of fresh, unweathered rocks. Chemical weathering of these fresh rock faces in turn removes carbon dioxide from the atmosphere. By this mechanism glaciation and periglacial processes (e.g. frost-wedging) may promote a positive feedback with global cooling by depleting the concentration of atmospheric carbon dioxide, leading to a "reverse greenhouse effect" (Raymo and Ruddiman, 1992). Understanding glacial erosion processes is thus vital to understanding Late Cenozoic earth surface processes and global climate change.

High altitude landscapes display spectacular features such as steep sided U-shaped valleys, cirques, and strings of paternoster lakes that are indicative of glacial erosion. Longitudinal profiles of glaciated valleys typically show flattened water- or sediment-filled

reaches separated by sharp, steep bedrock steps. The valleys typically terminate in cirques – amphitheater-shaped bedrock recesses that are located at the heads of glacial valleys. Cirques are characterized by a relatively steep arcuate headwall and a floor that consists of a rock basin enclosed by a small ridge or lip, known as a riegel. It has been proposed, based on observations of progressive glacial erosion, that the rate of horizontal backwearing at cirques is greater than their vertical incision rate (Brocklehurst and Whipple, 2002, Oskin and Burbank, 2005; Brook et. al, 2006; Naylor and Gabet, 2007) (Figure 1). Using an erosional unconformity surface, Oskin and Burbank (2005) reconstructed the landscape evolution in the Kyrgyz Range, a rapidly uplifting mountain range in the Tien Shan of Central Asia, and found that headwall retreat was approximately three times faster than downward erosion into the cirque floor. Similarly, by comparing a topographic analysis of north-facing glaciated valleys to south-facing fluvial valleys in the Bitterroot Range in Montana, Naylor and Gabet (2007) found that the ratio of lateral to vertical erosion by these alpine glaciers was roughly 4:1. Thus, the headward expansion of cirques may be the dominant form of glacial erosion, and thus it is particularly important to understand the processes responsible for cirque formation and expansion.

Ice Flow and Distribution of Erosion

Because basal ice velocity forms the basis for existing glacial erosion rules (Hallet, 1979, 1996), the problem of cirque erosion requires a basic understanding of glacial form and mass balance. Glaciers are characterized by three distinct sections: the accumulation area, where accumulation of ice from snowfall, avalanching, etc. exceeds ice loss; the ablation area, where melting, sublimation and calving contribute to a net loss of mass; and the equilibrium line, which is the line of demarcation between the two areas. The bergschrund is

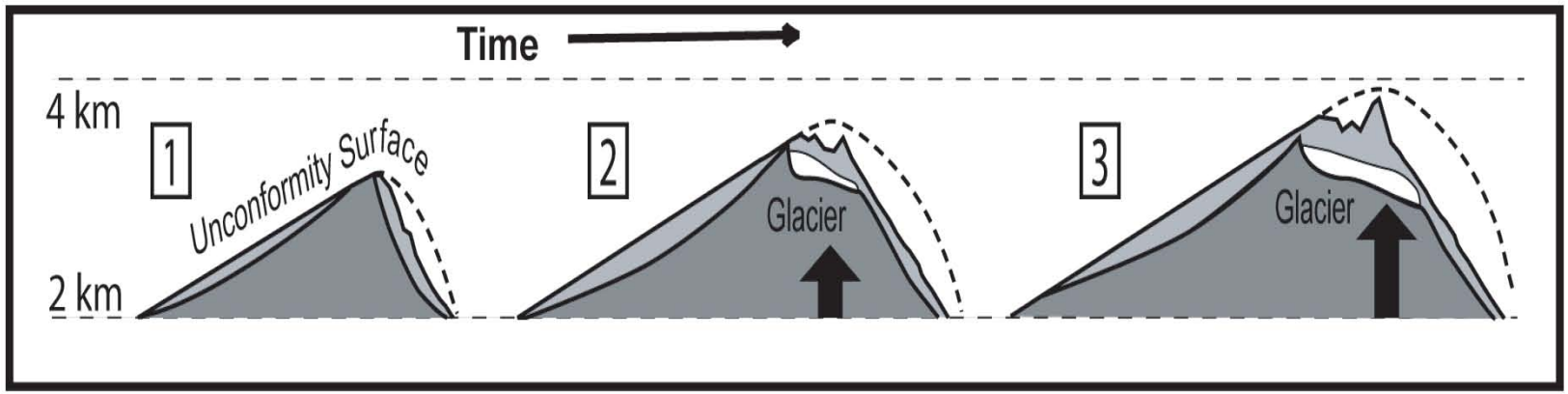

Figure 1
Glaciers erode horizontally more quickly than vertically.
Light gray denotes ridgeline elevation; dark gray represents valley elevation in the Kyrgyz range, an uplifting mountain range. (Modified from Oskin and Burbank, 2005)

a large crevasse that forms at the head of the glacier between the actively flowing part of the glacier and the uppermost stagnant ice that is frozen to the headwall.

Glacial ice flows from the upstream accumulation area to the downstream ablation area via two main mechanisms: (1) basal sliding, where the lubricated basal ice rigidly slides across the bedrock, and (2) internal deformation, where the ice column deforms and flows downhill under its own weight. There are different levels of deformation flow: dislocation creep at very high stresses; superplastic flow, where a crystalline material is deformed beyond its usual breaking point; basal slip; and diffusion flow at extremely low stresses (Goldsby and Kohlstedt, 2001; Marshall et al., 2002). Only basal sliding contributes to erosion of the bedrock floor, and in temperate climates sliding is generally reduced in the winter months when the ice is frozen to its bed, and flow is by deformation only (Hooke et al., 1989). In addition to down valley movement, the ice also flows relatively downward from the surface toward the base due to basal melting and compaction under younger layers of snow in the accumulation area (Reid, 1897). Conversely, melting of the ice surface drives flow relatively upward toward the surface in the ablation area. Both the maximum thickness and basal ice velocity occur at the location below the equilibrium line altitude of the glacier.

Glaciers physically remove rock material from mountains by abrasion, quarrying and sub-glacial water flow. Abrasion is the removal of silt-sized particles from debris-filled ice scraping across the bed, and quarrying is the removal of larger blocks of bedrock due to the stresses induced near cavities (Figure 2). There are a few generally accepted models of mechanical glacial erosion; although the physics behind these models are different, they all imply that erosion will intensify down glacier where ice flux is greatest near the location of the ELA (Boulton, 1974; Hallet, 1979; Anderson et al., 2006). If the models accurately and

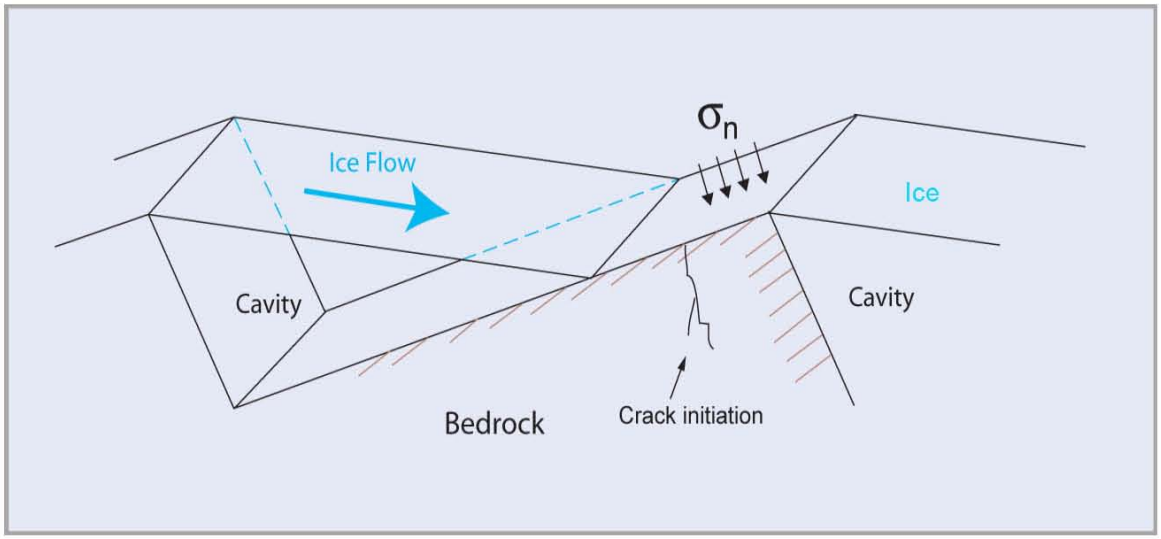

Figure 2
Higher water pressure causes ice-bed separation and the elevated normal stress on lee side of cavities causes fracture propagation in bedrock. Quarrying occus when fractured blocks of bedrock are removed and entrained in basal ice. Modified from Hallet (1996)

completely described glacial erosion, maximum erosion would be expected at the location of the long-term average equilibrium line altitude (ELA), instead of the enhanced erosion at the headwall that has been observed (Oskin and Burbank, 2005; Naylor and Gabet, 2007).

Mechanisms for cirque retreat

To understand what causes cirque retreat, it is necessary to define the processes that work to undermine the base of the cirque headwall, subsequently causing mass wasting and backwearing. By evaluating the individual features that affect differential erosion in cirques such as the overdeepening, the bedrock riegel, or the semi-circular headwall, a better conception of cirque processes may be attained. The formation of a riegel, the transverse bedrock ridge on the down-valley side of a cirque, may be a controlling factor in cirque formation and expansion. According to Hooke (1991) these transverse ridges in glacial valleys may constrict down-valley sub-glacial water flow, preventing ice from sliding at that location, and encouraging deposition of till in the downstream portion of a cirque basin (Figure 3) (Alley et al., 2003, Hooke, 1991). This process could prevent erosion of the cirque floor at that point (Hallet, 1979), but does not restrict erosion back into the headwall, thus indirectly facilitating cirque retreat. However, in order for this mechanism of cirque retreat to operate, the development of the riegel itself needs to be understood.

A possible explanation for riegel formation is that it develops over time from fluctuating levels of alpine glaciation (Figure 4). At the onset of glacial erosion into preexisting topography, an arcuate cirque will begin to form, although it does not initially possess a well-defined lip. When a valley is fully occupied by a glacier, flow out of the cirque will be only weakly convergent, the headwall will become increasingly curved and continuous down-valley ice flow will lead to the formation of a U-shaped valley (Harbor, 1992). During times

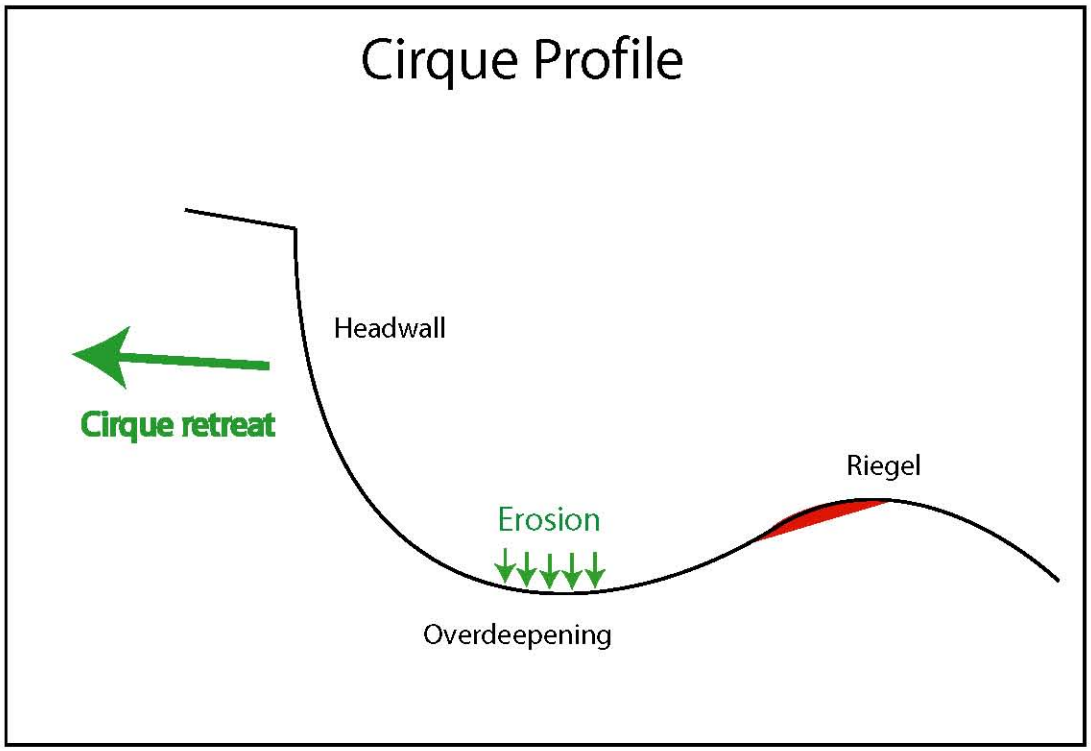

Figure 3
Presence of riegel may lead to positive feedbacks with overdeepening formation. Sub-glacial meltwater flow is restricted at location of perturbation, leading to till deposition and prohibiting erosion at that point (red). Enhanced erosion behind perturbation may form overdeepening and facilitate cirque retreat via mass wasting at the headwall (Hooke, 1991).

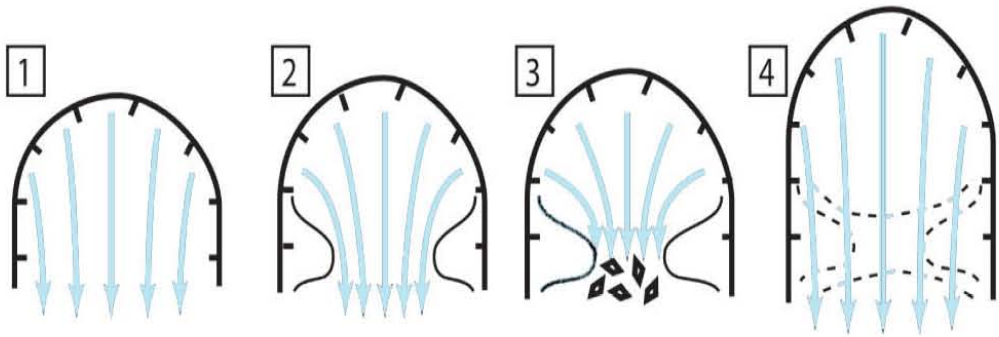

Figure 4
Conceptual model for formation of riegel by fluctuating levels of ice occupation and erosion
1. At onset of glaciation; weakly convergent flow into existing topography forms U-shaped valley and rounded headwall. No riegel is present.
2. Waning glaciation. Enhanced convergence in center of valley differentially erodes the middle forming shoulders.
3. Minimal glacial occupation deposits terminal moraine between shoulders.
4. Return to high occupation. Formation of overdeepening and riegel sets off positive feedback; backward expansion of cirque (Hooke, 1991)

of intermediate occupation by glaciers, convergent flow will be enhanced, and thus erosion is concentrated near the center of the channel at the valley head, leading away from the cirque. Differential erosion of this channel will in turn cause ‘shoulders’ to begin to form near the edges, a feature that is commonly observed on topographic maps of incipient cirques. When ice occupation is lowest, the glacier will retreat into its cirque and form a terminal moraine by depositing till between the shoulders. Upon return to full glacial conditions, this moraine and the adjacent bedrock shoulders inhibit glacial erosion at that point and contribute to enhanced erosion behind the moraine, forming a riegel.

This thesis describes how the hypothesis was tested by (1) studying a field example of a glaciated landscape and (2) implementing a simple numerical model to explore glacial erosion patterns. An analysis of morphometric characteristics taken in the field study indicate the cirques represent a progression in form and that perturbations such as riegel may grow through time. Highly variable striae orientations correlate to locations of thick ice and possibly lead to enhanced erosion in the center of valleys and formation of shoulders. The numerical model shows that a constriction may produce conditions favorable for formation of an overdeepening, but only when the quarrying erosion rule includes a threshold gradient.

Background

Cirque Erosion

From the earliest studies of cirque genesis, researchers have attempted to explain the morphology of cirques through time. From field observations, cirque form was found to have initiated from the gradual accumulation of snow in nivation hollows (Matthes, 1900; Johnson, 1904; Rapp, 1984), which are small depressions formed and perennially occupied by snow. These studies have raised questions regarding the end product of cirque erosion. Some morphometric analyses indicate that cirque form reaches equilibrium, with larger cirques being better developed and more concave (Haynes, 1998; Evans and Cox, 1995), whereas others indicate that cirques continually increase in length and degree of overdeepening (Garcia-Ruiz et al., 2000; Brook et al., 2006). These latter studies are supported by observations that large-scale cirque retreat constitutes a majority of glacial erosion across some mountain ranges (e.g. Oskin and Burbank, 2005; Naylor and Gabet, 2007).

From tunnels at the base of a cirque glacier in Norway, McCall (1972) identified rotational sliding motion, and found shattered blocks at the bergschrund and an armoring layer of till below the glacier, which led to the conclusion that backwearing of the headwall was a dominant mechanism of cirque expansion. This field evidence is consistent with Hooke's (1991) field and theoretical work in which it was postulated that quarrying would be greatest downvalley from both the bergschrund and any transverse bed perturbations, above

which crevasses act as a conduit for surface water to reach the bed. The resulting water pressure fluctuations create unstable basal stresses, which lead to crack propagation and enhance quarrying of the bedrock. Erosion is impeded near riegel because the upward flow of supercooled sub-glacial meltwater causes sediment deposition and restricts erosion at riegel crest. A positive feedback is initiated, where overdeepenings will become deeper, perturbations more prominent, and cirques expand.

Glacial erosion rules

To garner a comprehensive understanding of the processes responsible for the formation, expansion, and subsequent retreat of cirques, it is necessary to examine in detail the currently accepted glacial erosion rules. In Boulton's (1974) model of glacial abrasion, the rate of erosion is directly proportional to the mean basal ice pressure, or the force at which a glacier presses an entrained rock particle against the bedrock surface, from the equation:

$$F_b = (\rho_i g h_i - P_w) A_i \tan\beta$$

Where F_b is the force on the bed, ρ_i is the density of ice, g is the acceleration due to gravity, and h_i is the height of the ice column. The basal water pressure is represented by P_w and the slope of the bed by $tan\beta$. A_i is a constant that includes ice temperature, debris concentration, and ice crystal orientations. Because the mean basal ice pressure depends upon ice thickness, h_i, he concluded that this force largely depends on the weight of the overlying ice. The ice thickness may be relevant in calculating erosion rates where the basal debris concentration is very high and the ice acts as a rigid slab, or where it prevents the rotation of abrading cobbles and therefore affects erosion rates (Iverson, 1989).

An alternative model, formulated by Hallet (1979), is based on the idea that the basal ice deforms completely around entrained rock particles, and thus it is the buoyant weight of the tools embedded within the ice that drives abrasion,

$$F_p = V_p(\rho_r - \rho_i)g$$

Where V_p is the volume of a rock particle and ρ_r is the rock density. This model suggests that ice thickness is mostly irrelevant when calculating glacial erosion rates because the force that causes abrasion depends on the buoyant weight of rock in ice. The integrated erosion rate will depend upon the number of particles impacting the bed, which in turn depends on the amount of debris entrained in the ice and the velocity at which ice flows toward the bed. As ice flows downward due to basal melting, it drags these buoyant rock particles and presses them into the bedrock, thus eroding by abrasion as the ice slides downvalley. The physics in Hallet's model were verified by laboratory experiments simulating glacial abrasion (Iverson, 1990).

Both Boulton's and Hallet's models imply that erosion is greatest at the location of the long term average ELA because both ice thickness and downward ice velocity are greatest there. Clearly, neither model provides an explanation for the significant amount of erosion that occurs at the heads of glacial valleys, where ice flux is at a minimum.

Modeling of Glacial Erosion

Several generations of numerical models have been used to elucidate the relationship of glacial flow and erosional processes to alpine geomorphology. Oerlemans (1984) was the first to quantitatively model glacial erosion. He used a simple rule for glacial erosion, incorporating both abrasion and quarrying to model large-scale features and the interaction between ice flow, erosion and lithospheric flexure. Harbor (1988, 1992, and 1995) used a

two-dimensional model to quantify the formation of U-shaped valleys from glacial occupation of initially V-shaped valleys. To study longitudinal profiles of glacial valleys, MacGregor et al. (2000) employed a one-dimensional finite-difference numerical model simulating the formation of glacial valley profiles and the overdeepenings that form due to increased ice flux at tributary junctions. Anderson et al., (2006) derived an analytical model for glacial valley long-profile erosion. They found that glaciers will erode a semi-parabolic longitudinal profile in the bedrock with maximum erosion at the location of the long-term average ELA, located at approximately 30-40% of the average length of the glacier.

None of the aforementioned models provide insight into the formation of localized overdeepenings that are found in cirques or the significant erosion that is observed at the headwall of alpine glaciers. A model that does consider these processes was formulated by MacGregor et al. (2009). These authors successfully simulated the formation of a cirque overdeepening, albeit only when glaciers were very small and quarrying was the major erosive mechanism near the headwall. In their model formulation the quarrying rate is proportional to the sine of local bed slope.

The modeling approach presented in this thesis does not directly assess the erosion processes at the head of a cirque glacier. Rather I focused this model on the development of riegel within a glacial valley profile. Understanding this process is important insomuch as these features, often located at the outlets of cirques, may indirectly favor cirque headwall retreat by promoting till armoring of the cirque floor (Hooke, 1991). My results show that a threshold slope for quarrying may be key to development of the steep down-valley wall of a riegel. A similar threshold may also act to focus quarrying and retreat of cirque headwalls. This slope-dependent quarrying approach is similar to that employed by MacGregor et al.

(2009). However a threshold, rather than a smooth sine function of slope, was needed to induce formation of abrupt headwalls down valley of riegel.

Field Study

To test the hypothesis that riegel, and consequently cirques, form from fluctuating levels of ice occupation, glacially eroded terrains were examined in the southern Sierra Nevada of California. Spanning over 600 km from north to south, between 35° and 40.5° north latitude along the east-central portion of California, the Sierra Nevada range is the remnant of an eroded Mesozoic batholith intruded into accreted island arc terranes and metamorphosed sedimentary rocks on the western margin of North America (Bateman and Eaton, 1967). Late Tertiary tectonic activity has uplifted the plutonic block and tilted it to the west; extensional faulting to the east is still presently active (Gillespie and Zehfuss, 2004). The Sierra Nevada rises to a peak elevation of over 4,400 meters, forming a steep escarpment on the eastern side where the Sierra Nevada Fault Zone represents the westernmost edge of the Basin and Range province. The range slopes more gently westward into the San Joaquin Valley.

The Sierra Nevada present a suitable field site in which to interpret cirque evolution from striae orientations because the exposed plutonic bedrock (Mathews and Burnett, 1965; Bateman, 1969) is structurally more uniform than layered volcanic, metamorphic or sedimentary rocks in other glaciated mountain ranges (Brocklehurst, 2004). Where the bedrock is granitic, cirque form can solely be attributed to glacial erosional processes. The possibility that rocks of differing lithologies and resistance to erosion influenced valley morphology (e.g. Augustinus 1988, 1992) may thus be disregarded.

Many of the glaciated landforms in the Sierra Nevada have been well preserved since the last deglaciation ca. 14 ka (Clark and Gillespie, 1996), with minimal post glacial freeze-thaw activity working to obliterate the geomorphic history in the landscape. Glacially weathered landscapes are generally characterized by smooth surfaces covered with grooves of various widths, lengths and depths. These grooves are known as striations, or striae, and they are left behind as debris-filled ice scrapes across the bedrock. Because they may indicate the local direction of ice flow down the valley their orientations have been used to infer the geomorphic and glacial flow history of a region (e.g., Kleman, 1990). In this study, the orientations of glacial striae were measured to infer the history of ice flow in three alpine cirques.

Of the many cirques in the Sierra Nevada, only those that met certain criteria were considered as candidates for detailed study. A digital elevation model (DEM) from the Shuttle Radar Topography Mission with 30-meter resolution and USGS topographic and geologic maps were examined to find an area in which several small (<1 km in diameter) cirques were isolated and accessible. The cirques had to have been carved entirely out of plutonic rocks; those within the metamorphic or volcanic pendants were avoided. For simplicity the chosen cirques are smaller than one kilometer in diameter.

The four cirques that were intimately examined, Tar Gap, Mosquito Lake, East Mineral Lake and West Mineral Lake, encompass an area of 5.7 square kilometers in the southern end of the Sierra Nevada, approximately 4.5 kilometers southwest of Mineral King in Sequoia National Park (Figure 5). The bedrock lithology is granodiorite (Mathews and Burnett, 1965). The cirques are found on north-facing slopes near the edge of glacially imprinted landscapes. This is evident because nearby catchments that are located at a comparable

altitude on south facing slopes exhibit evidence of fluvial erosion only, with parabolic river profiles and V-shaped valley cross sections. As many other locations in the Sierra Nevada are located at higher elevations and have likely had multiple, extensive glaciations, it is plausible to assume that the cirques present in this area represent relatively early forms of glacial landscape evolution.

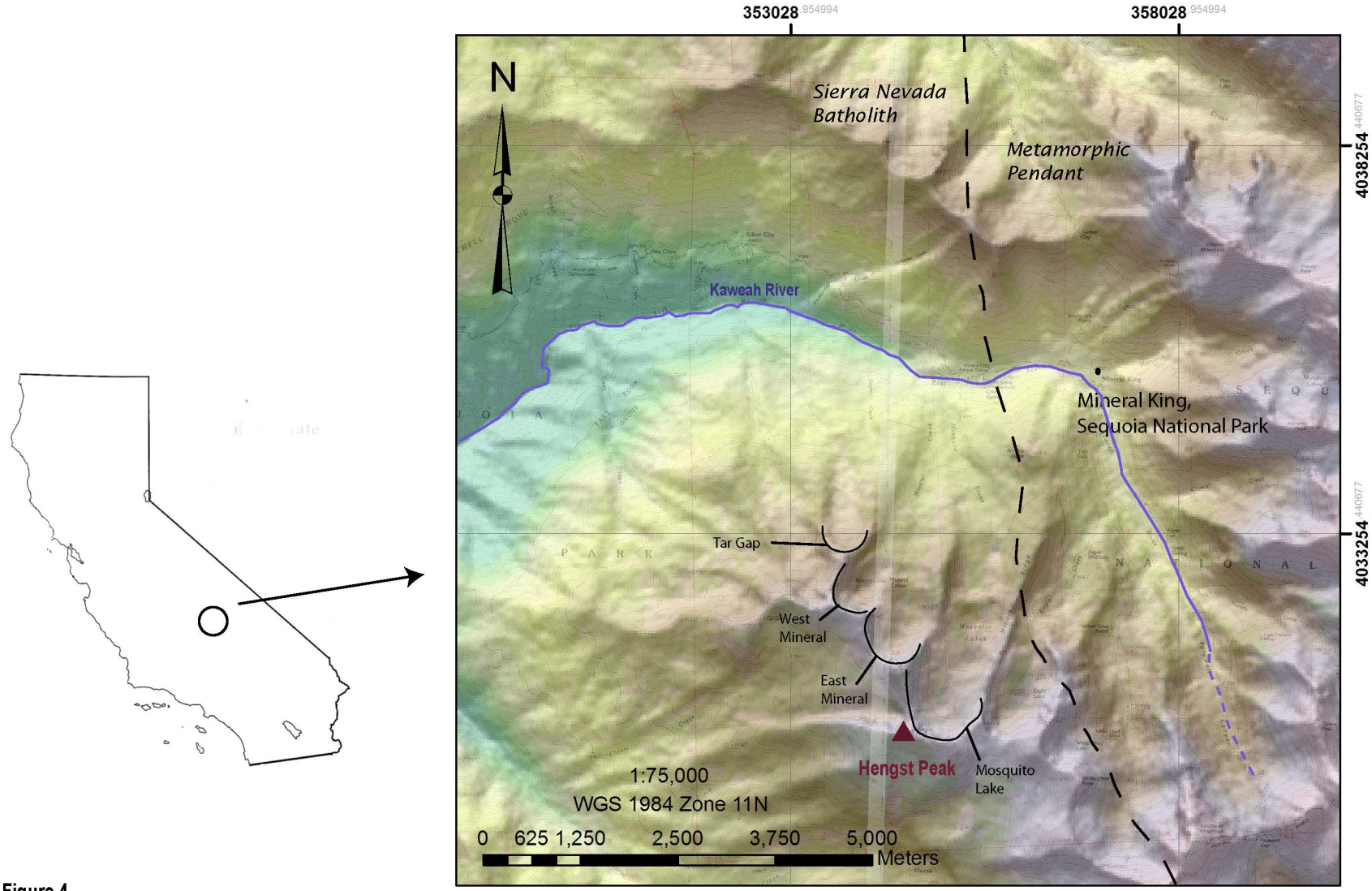

Figure 4
Map showing location of field study area in the Sierra Nevada, California. Individual Hengst Ridge cirques are highlighted. South-facing drainages north of Kaweah River valley are fluvial; north-facing drainages are glaciated. Dashed line delineates plutonic Sierra Nevada Batholith rocks from metamporphic.

Methods

Measurement of striae

The three glacial valleys (Mosquito, East Mineral and West Mineral) were thoroughly examined to find evidence to provide insight toward the hypothesis that fluctuating levels of glacial occupation lead to the formation of cirques. Striation plunge angles and directions were measured using a Brunton pocket transit compass. The compass was aligned parallel to the striations and the orientation recorded in degrees. Ice flow directions were assumed to be positive in the down-valley direction, consistent with the abundant chatter marks preserved in the field area. The relative ages of striations were noted, according to the standards outlined by Janssen et al. (2002): (1) where two sets of striae are found on a single surface, the striations on the lee side of other striae sets are younger, (2) striations on crests between large grooves and coarser striae are younger, and (3) striations cutting across other striations are younger. In an attempt to keep a relatively evenly spaced data set with continuous coverage, striae orientations were measured on exposed bedrock every thirty to forty meters, where possible, in a grid-like pattern throughout each cirque, from the headwall to well below the riegel. The precise location of each measurement was determined using GPS units with an accuracy of less than ten meters. The GPS was connected to a hand-held field computer and orientation data entered as it was collected.

Geomorphic mapping

Glacial geomorphology was mapped on aerial photos, with particular attention paid to ridges and steps not indicated on existing DEMs or topographic maps. Riegel, steps, cirque headwalls, and till were all observed and noted on the field maps. Trim lines marking the maximum extent of glaciation were mapped for the entire field area based on the locations where soil-mantled surfaces met exposed striated bedrock and moraines. These field maps were then compared to a map of slopes calculated in ArcGIS from the 30 meter SRTM digital elevation model and trim lines were inferred at prominent slope breaks, after the methods of Brocklehurst (2002).

Morphometry

Morphometric measurements were taken remotely using topographic maps and orthophotos in ArcGIS. Although it was not included in the field data collection, Tar Gap cirque is included in the morphometric analysis, as it is located at a lower elevation on the same ridge as the three cirques studied in the field. Cirque development was quantified by measuring the distance across valley transect, overall relief from headwall to overdeepening; elongation of cirque, measured as ratio of length to width; and basin and headwall elevation. Topographic profiles were taken along cirque axes and riegel to compare degree of overdeepening and maximum and minimum gradient.

Numerical Model Setup

To understand the sub-glacial erosive processes that act at the heads of glaciated valleys and cause cirque retreat via mass-wasting of the headwall, a simple one-dimensional finite difference numerical model was formulated, similarly to many previous models that link ice flow, glacial erosion and valley form to explore the development mechanics (e.g. Oerlemans,

1984; Harbor, 1992; MacGregor et al., 2000; MacGregor et al., 2009). It was formulated to test the hypothesis that the presence of bedrock "shoulders" can set off a positive feedback reaction which will create an overdeepening and cause cirque expansion and headwall retreat. Unlike previous models, it does not simulate erosion over an entire glacial valley, nor was it written to specifically simulate cirque erosion. Instead, the model replicates the effect that a small glacier would have on the bedrock topography over one location in an alpine valley. By addressing the erosion at work near the riegel, the model sheds light upon the processes that are acting at the heads of glaciated valleys, particularly how the bed is eroded when ice flows over a perturbation or through a constriction in a valley.

Although multiple parameters could be varied, some initial conditions were set and remained fixed through almost all model simulations presented here. The model is one dimensional, but set up in a rectangular coordinate system with the independent x-axis in the downvalley ice flow direction, the dependent z-axis is the bed elevation or ice height, and the y-axis is the fixed unit width of the valley. Many of these initial shape parameters were tested, but the simulated valleys presented in this thesis have a specified length of 5000 meters and a 10% gradient, split into 5 meter increments. To simulate a sharp constriction in some model runs, a friction factor of 0.5 multiplied by the sinc function raised to the fourth power $\left(\frac{\sin \pi x}{\pi x}^4\right)$ was applied.

A fixed ice flux of 1000m^2/yr is used with periodic boundary conditions: ice exiting the system is recycled as ice input into the system. There are two components of ice motion in a valley glacier: motion due to internal deformation (U_{def}), which involves internal movement of ice crystals relative to one another, and motion due to basal sliding (U_{slide}). The driving force for ice flow, both by deformation and sliding, is the driving stress (τ_d) which is a

function of ice thickness, or height (h_i) and surface slope (α), along with the density of ice (ρ_i) and acceleration due to gravity (g):

$$\tau = \rho_i g h_i \sin\alpha$$

To model deformation, the relationship of strain rate to stress is described by Glen's Law (Glen, 1955):

$$\varepsilon_{eff} = A\ \tau_{eff}^{n}$$

where ε_{eff} represents the effective strain rate and A is a temperature-dependent constant. A mean value of 3 is often assigned to the exponent n based on laboratory and field observations (Paterson, 1994 p. 85), indicating that the strain rate of an individual unit of ice increases exponentially as the ice overburden, or thickness, increases. Using Glen's Law yields an expression for the flow of ice in a column due to internal deformation:

$$U_{def} = {}^{2}/_{5}\ A\ (\rho_i g h_i \sin\alpha)^3$$

Each model year is separated into summer and winter over 800 – 1200 steps per model year. During the model winter the glacier is frozen to the bed (Hooke et al., 1989), and ice moves solely via internal deformation; during the model summer, when the beds of glaciers are lubricated by melt water, ice moves due to both sliding and internal deformation. As glacial erosion is dependent on sliding velocity, (Hallet, 1979; Iverson, 1991; Harbor, 1992; Hallet, 1996; Alley et al., 1999) erosion only occurs during model summer. The sliding rule is similar to that employed by MacGregor et al. (2001, 2009) where C is a constant based on temperature and mechanical properties of ice and bed roughness (Paterson, 1994 p. 152):

$$U_{slide} = C * \rho_i g h_i \sin\alpha$$

The equations used to model erosion are based on the work of MacGregor et al. (2009); however because the intent here is to model the mechanics of glacial erosion after varying

the initial bed geometry, debris entrainment, clast comminution, and sub-glacial water pressure were not included in these rules. Abrasion and quarrying are treated separately in this model. The rule for erosion by abrasion-only (ε_{abr}) is:

$$\varepsilon_{abr} = C_{abrasion} * U_{slide}$$

with sliding velocity as the only defining parameter from theoretical erosions models (Hallet, 1979) and field observations correlating sliding speed to erosion rates (e.g. Humphrey and Raymond, 1994; Riihimaki et al., 2005). It has also been postulated that sliding speed controls quarrying rates because the size of sub-glacial cavities increases with basal ice velocity, and pressure differentials lead to plucking (Cohen et al., 2006). The quarrying erosion rule is a simplified version of the rule recently developed (MacGregor et al., 2009); the slope of the bed is included in this term because quarried surfaces are found only on the lee sides of asymmetric glacial landforms:

$$\varepsilon_{quarry} = C_{quarry} * U_{slide} * \sin\beta$$

Where ε represents the erosion rate, U_{slide} is the sliding velocity, and β is the slope of the bed. It was necessary to incorporate an additional parameter to the erosion rule: a threshold gradient must be reached before quarrying commences, and erosion is by abrasion only until the alley attains a slope of 12.5%. This factor was guided by the difficulty of producing stepped topography with the simple conservative rules previously used, as well as field observations of steep quarried lee sides of riegel. The values for each erosion coefficient (C_{quarry} and $C_{abrasion}$) were guided by field data comparing the relative rates of abrasion to quarrying (Hallet et al., 1996; Briner and Swanson, 1998), although different ratios of C_{quarry} to $C_{abrasion}$ were tested, and for efficiency of the model, higher values were sometimes employed.

Results

Measurements of Striae

Striations and glacial polish are ubiquitous in all three cirques (Figure 6). Glacially abraded surfaces are found from the lowest point in the valley center to the high ridges that separate each drainage basin, and extend from the base of the headwall in the cirque overdeepening down valley to the uppermost tarns. Striations are scarce lower in the glacial valleys. The majority of striae are well preserved and likely record ice flow during the most recent, Tioga, glaciation that culminated approximately 14 -15 ka (Clark et al., 2003). Some striated surfaces high on the valley walls and on bedrock benches on the valley sides are covered by a darker patina. These surfaces are rougher to the touch and have inferior striae preservation, as they seem to be more chemically abraded than the smooth, polished, and heavily striated surfaces near the center of the valley axis. Small (<1cm wide) striations are abundant on the polished bedrock at the valley axis, whereas the grooves found on the rough, weathered surfaces at higher elevations along the sides of the cirque are often wider and deeper.

In only a few locations did striations appear to be preserved from multiple glaciations. Some overprinted and diverging striae were found on the tops of the ridges dividing drainages. Additional evidence for multiple glaciations is preserved at lower elevations, within the cirque. Here larger, deeper, and rougher grooves show trends that deviate from those of the numerous smaller striations found on the same bedrock surface (Figure 6).

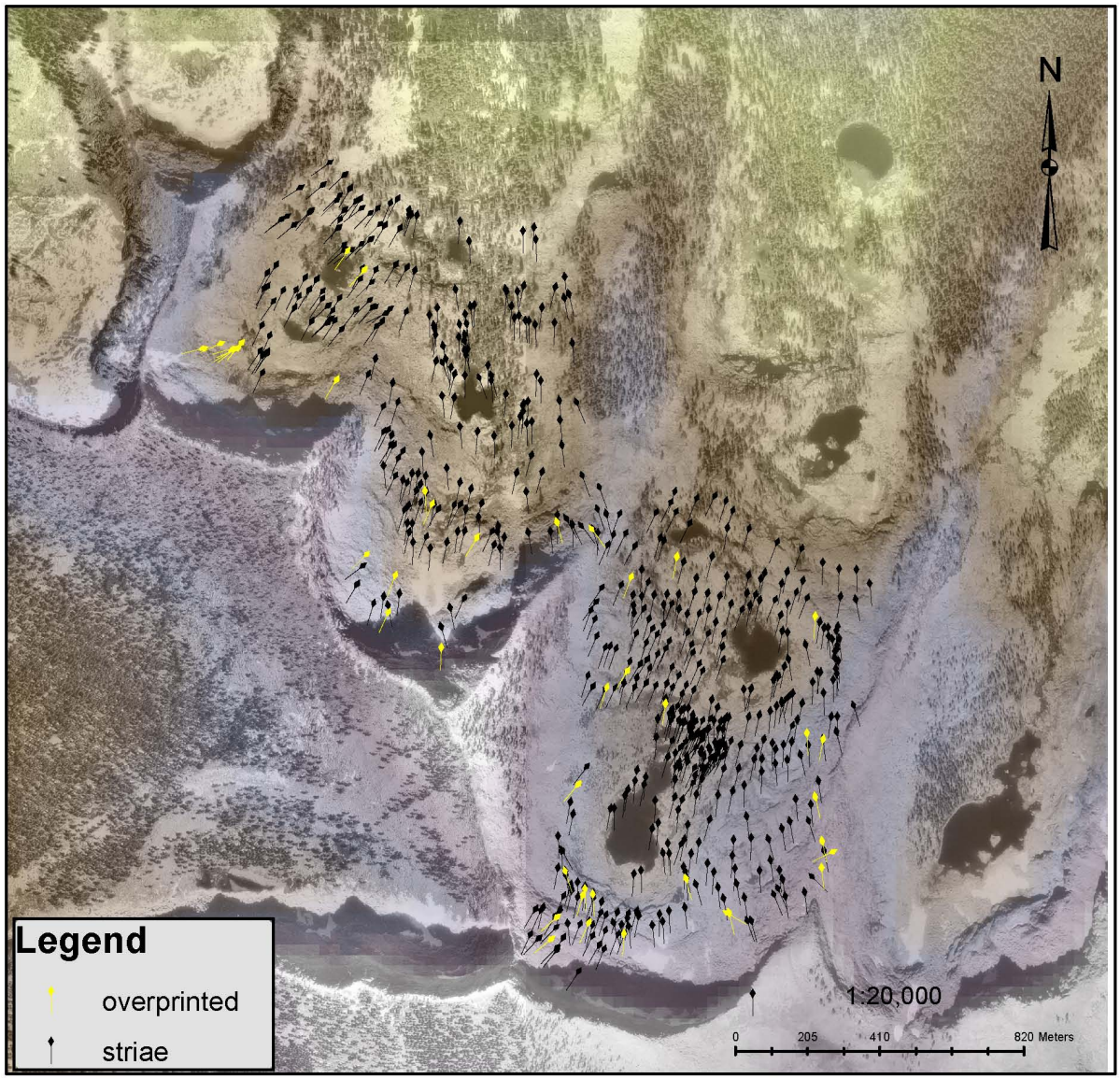

Figure 6
Map of Hengst Ridge cirques showing striation orientation data collected. Overprinted striae are highlighted in yellow.

Morphometry

Quantifying the morphometry of the cirques highlighted possible trends in cirque form (Figure 7). Observations of increased closure and riegel development in the field and on digital elevation models, aerial photos and topographic maps indicate that the cirques exhibit a progression of both size and form from west to east. The aspect of all cirques is north-northeast, and the ridge that comprises the cirque headwalls trends northwest – southeast. The maximum elevation of the ridge increases from west to east. The elevation of the cirques steadily increases from west to east, with Tar Gap cirque at 2820 meters, West Mineral Lake cirque occupying an elevation of 2945 meters, East Mineral Lake cirque is at an elevation of 3000 meters, and Mosquito Lake cirque is at 3055 meters. Elevation measurements were taken from the cirque lip, after the methods of Trenhaile (1974). The area of each cirque also increased from west to east and the length to width ratio of the Mosquito Lake cirque is greater than the western cirques, whereas the maximum relief of the cirques varies, from 335 meters in Mosquito Lake, 360 meters in East Mineral Lake, 310 meters in West Mineral Lake and 316 meters at Tar Gap. Profile graphs drawn along the axis of each cirque from the headwall to beyond the cirque lip indicate that the degree of overdeepening and profile concavity steadily increase from Tar Gap to Mosquito Lake cirque (Figure 8). West Mineral Lake cirque, the most westerly of the three, has only a small polished riegel located downvalley of a relatively shallow overdeepening, whereas Mosquito Lake cirque, the most easterly, has a large, well defined bowl-shaped depression bounded by a prominent riegel. A map of slopes throughout the study area shows the gentle floor gradient that characterizes the Mosquito Lake valley, and the relatively steep slopes in the

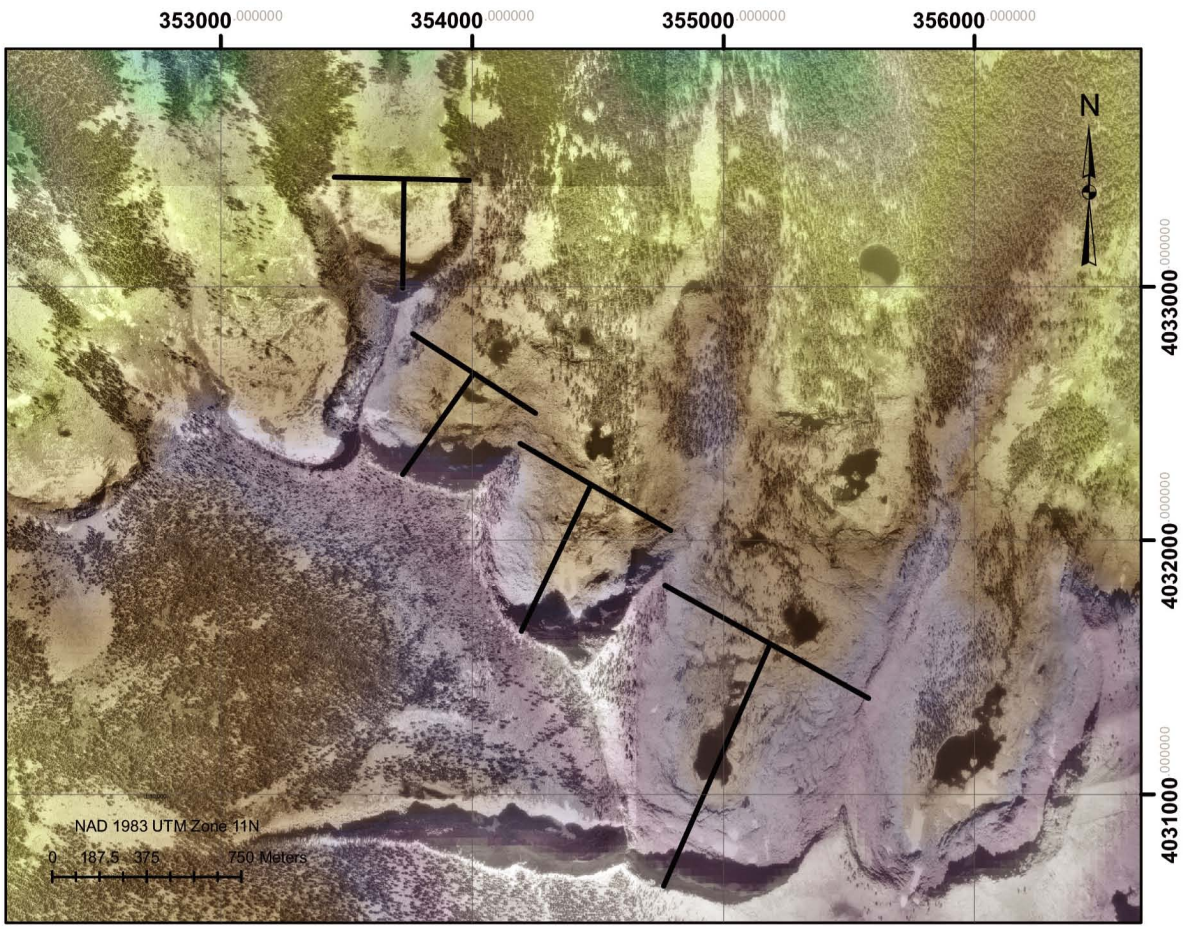

	Tar Gap	W Mineral	E Mineral	Mosquito
width (km)	0.540	0.570	0.710	1.040
length (km)	0.450	0.500	0.625	0.940
elongation (l/w)	0.833	0.877	0.880	0.904
peak elevation (m)	3136	3250	3360	3392
cirque elevation (m)	2820	2940	3000	3053
relief (m)	316	310	360	339

Figure 7
Morphometric characteristics measured in each cirque. Map shows length and width of cirques. Cirque elevation was measured from lip downvalley of first overdeepening. Relief measurements do not account for depth of lake-filled overdeepenings.

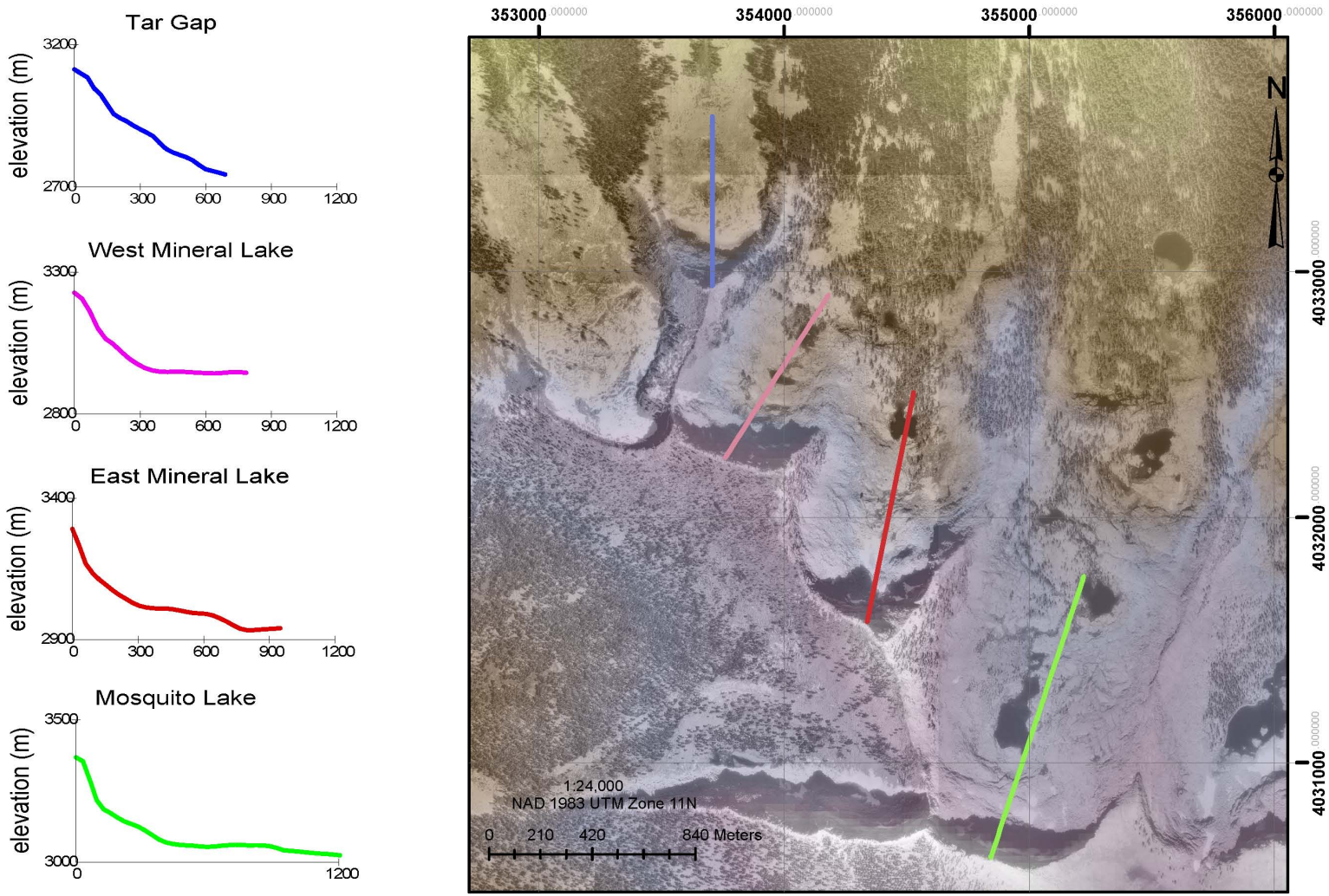

Figure 8
Elevation profiles taken from the headwall to well below the riegel of all four cirques in study area. Cirques exhibit a progression in degree of concavity from Tar Gap in the west to Mosquito Lake in the east. Tar Gap has no overdeepening, and Mosquito Lake has a distinct overdeepening. The Mineral Lakes exhibit intermediate concavity.

Tar Gap valley (Figure 9). Additionally, graphs along cirque axes of slopes reveal maximum gradient in the Mosquito Lake cirque is greater than the more westerly cirques.

Geomorphic Mapping

Geomorphic mapping of the Mosquito Lake Valley revealed multiple step-like benches on the eastern side of the valley, similar to those observed in glaciated valleys in the northwestern Sierra Nevada (James, 2003), and a large area covered by till on the western side (Figure 10). The aspect of this slightly elongated cirque is north-northeast. Like most other glacially carved alpine valleys, the Mosquito Lakes Valley is characterized by multiple steps and overdeepenings. There is a succession of six small lakes (the 'Mosquito Lakes') occupying bedrock overdeepenings progressively down-valley from the cirque headwall. The positions of these lakes also alternate from the eastern to the western sides of the valley. Mosquito Lake 6 occupies the highest overdeepening with a surface elevation of 3055 meters. Mosquito Lake 1 is the furthest down valley, at an elevation of 2763 meters. Each lake-filled overdeepening is followed by a transverse bedrock ridge, or riegel. Very steep, high-relief cliffs with abundant evidence for erosion by plucking occur immediately down valley of each riegel. Striations and glacial polish are abundant and extend from the headwall base and sides of the cirque down to Mosquito Lake 3.

The Mineral Lakes valleys consist of two cirques, East and West Mineral Lakes, which are described and mapped together in this analysis (Figure 10). The Mineral Lakes valleys encompass of a total of five small lakes. Striations are plentiful, especially near the smooth overdeepened area in the centers of the valleys, although they are not as abundant as in the Mosquito Lakes cirque. East Mineral Lake cirque has an irregular hummocky upper overdeepening which is not as conspicuous as the lower overdeepening that contains the

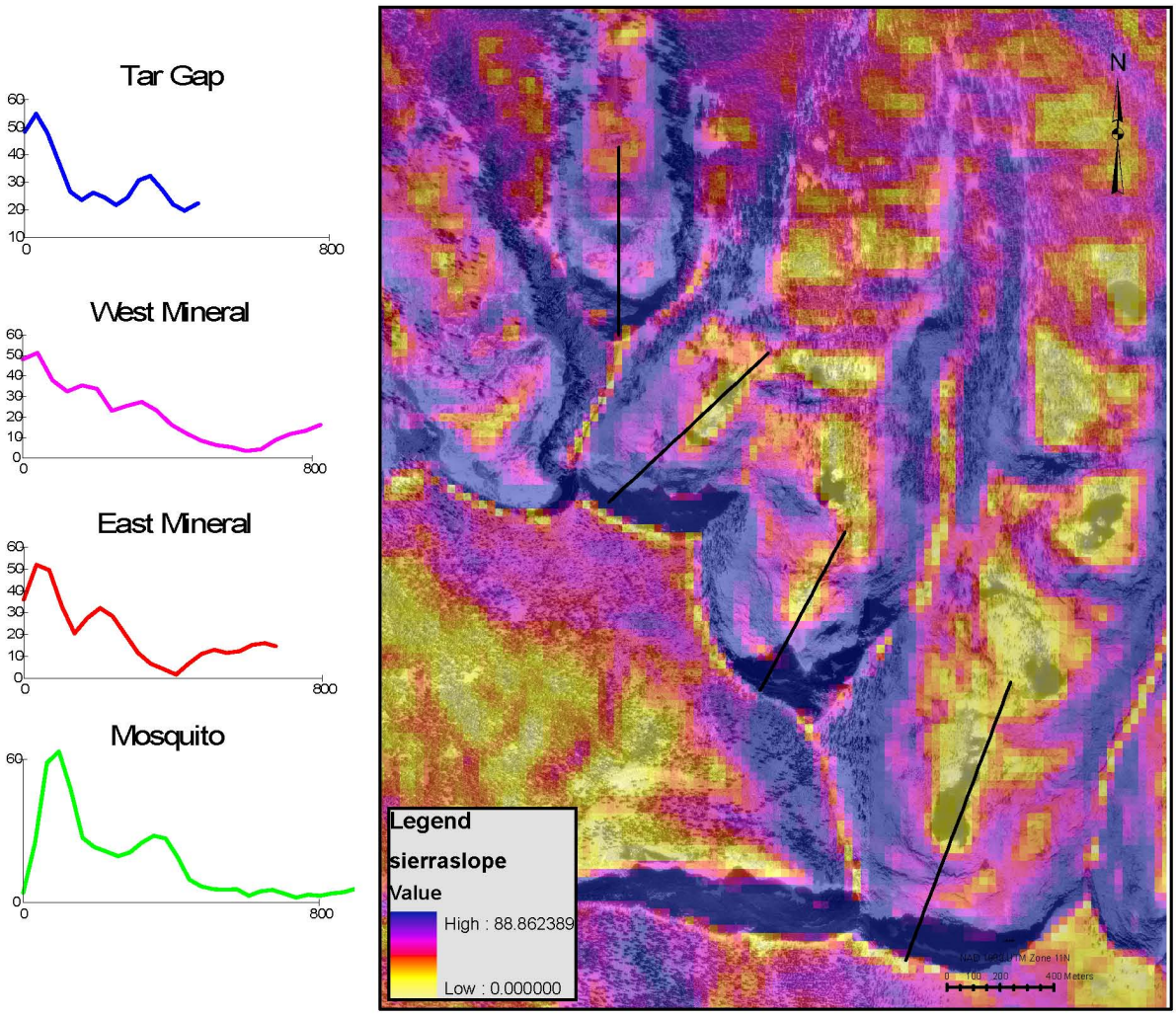

Figure 9
Map and graphs of slopes in Hengst Ridge area. Blue denotes high gradients; yellow are low. The Mosquito Lake valley has a very gently sloping floor, the Mineral Lakes valleys have intermediate slopes and the Tar Gap valley has relatively steep slopes, indicating that cirque maturity increase from west to east across the study area.

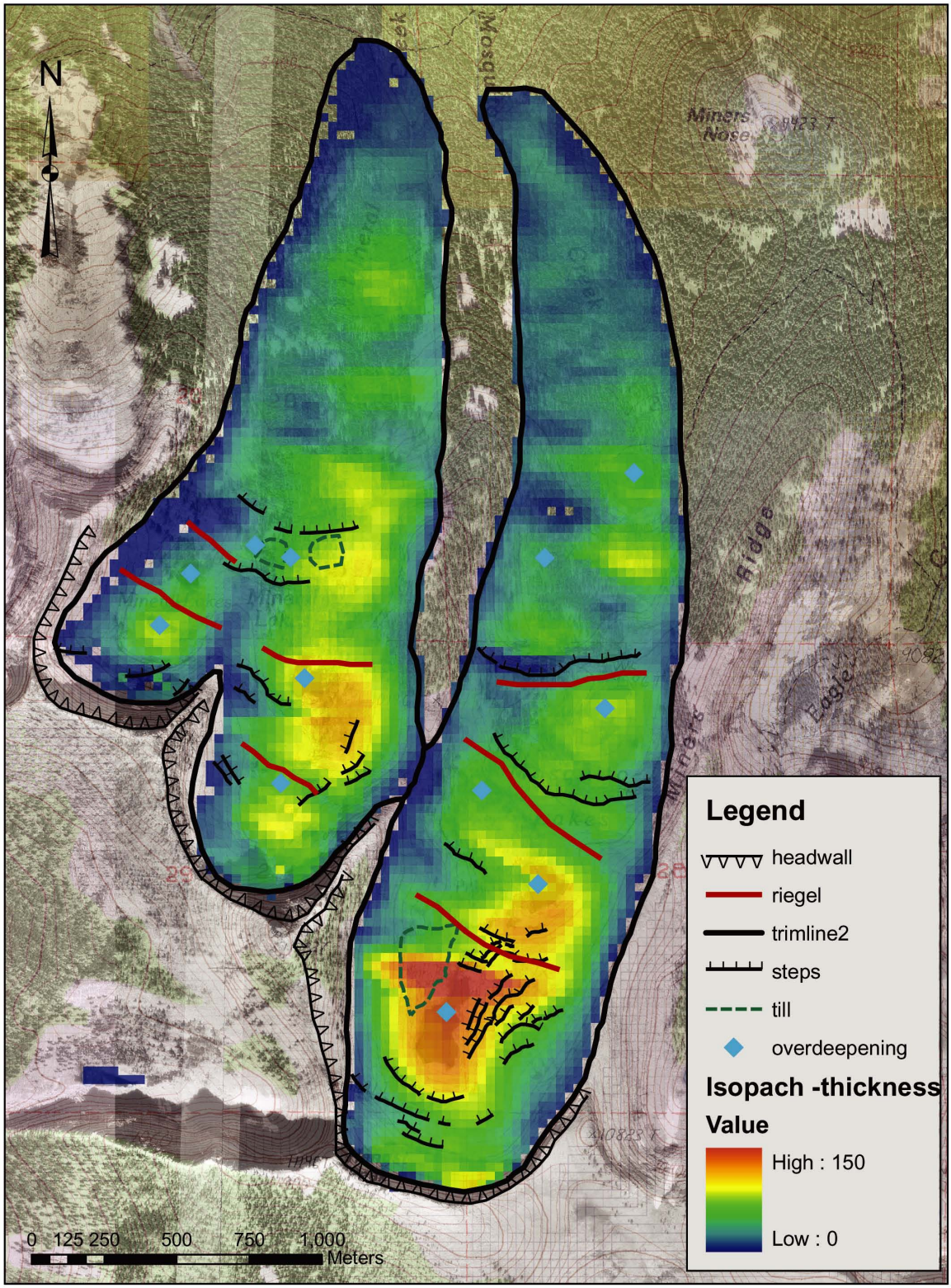

Figure 10
Geomorphic map of East and West Mineral Lakes and Mosquito Lakes valleys with ice thickness calculated from trimline elevations.

main lake. The East Mineral Lake valley contains fewer lakes than the Mosquito Lake cirque. The overdeepenings exhibit a slightly meandering pattern, similar to the pattern seen in the Mosquito Lakes cirque, but less pronounced. West Mineral Lake cirque has a very small overdeepening occupied by a relatively shallow pond. The two Mineral Lakes cirques merge, forming one glaciated valley downstream.

In addition to the topographic features in each cirque, glacial trim lines were mapped, thus providing information about the glaciers that previously occupied the three cirques. The error in trim line mapping is approximately 20 meters. A triangular irregular network (TIN) was calculated in ArcGIS by interpolating between trim line elevations to derive a paleo-surface for the preexisting glaciers. Because glacial surfaces are generally convex upward in cross profile downstream of the ELA, and concave upward upstream of the ELA, this TIN surface represents the maximum surface elevations in the uppermost reaches of the valleys. By subtracting the base 30-meter resolution DEM from the TIN, thickness maps, or isopachs, were then calculated, thus revealing the maximum depth of the glaciers (Figure 11). Negative thickness values represent locations where the base elevation was greater than the trim line TIN. These occur near the toe of the reconstructed glaciers. The maximum ice thickness values in each cirque progressively increase from west to east. The thickest section of the Mosquito Lake glacier, at the location of the cirque overdeepening is ~190 meters thick. The maximum thickness of the East Mineral Lake glacier is ~110 meters thick, and the West Mineral Lake glacier is ~80 meters thick. These thicknesses do not include the depths of the lake-filled portions of cirque overdeepenings.

Numerical Model Results

Numerical modeling was used to gauge how glacial erosion could produce the characteristic step-like topography of glaciated valleys. The approach taken here was to investigate how various perturbations in valley floor topography were either enhanced or removed by erosion. The purpose of this project is to investigate the mechanics and feedbacks associated with glacial erosion on and near an incipient riegel, so only those parameters that affect flow and erosion near a bedrock bump or constriction are tested. Presented here are the results of several simulations that test the mechanics of erosion at the riegel by modeling ice flow (1) over an initial perturbation in the bedrock topography and (2) around the bedrock shoulders that constrict the width of a valley. Because neither model could enhance the sharp, step-like features of glaciated valleys, a third set of models was run with a modified, threshold-based rule for glacial plucking.

Linear glacial erosion with perturbation

The first model run simulates a transverse perturbation at the midpoint of the 5-kilometer section of a glaciated valley. The maximum perturbation height is 15 meters, located on the node at the halfway point of the valley. The form of the perturbation is a sinc function ($\frac{\sin \pi x}{\pi x}$) raised to the 4^{th} power. This creates a somewhat peaked perturbation of the valley floor that decays smoothly away from the center of the model. Variables that were tested were the length of the valley section, height of perturbation, and slope of initial bed profile. However, in all perturbation simulations, regardless of the height of the initial bump or the slope of the initial valley, the perturbation is eventually smoothed away. Initially, the ice thickens and reaches a maximum just before the location of maximum perturbation (Figure 11). The ice flowing over the valley floor then gradually erodes into the floor and

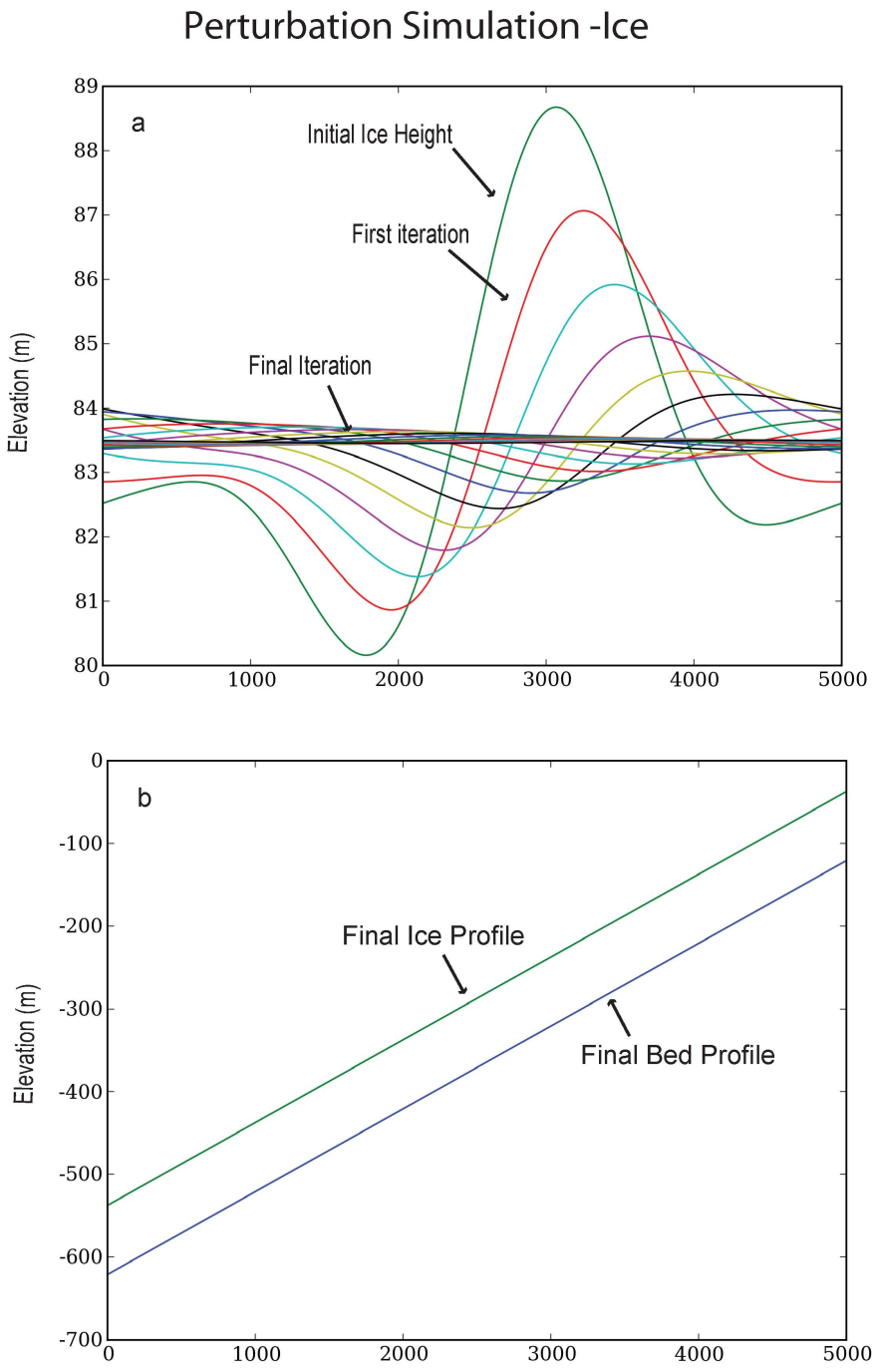

Figure 11
Perturbation simulation. (a) Ice initally piles up behind the perturbation, but it is quickly eroded away. (b) The final profile is a smooth linear valley.

obliterates the perturbation (Figure 12). After each model iteration, the slope of the valley floor and the ice height both systematically decrease. In the final model step, the valley exhibits a level, linear profile, with a slope matching the initial valley slope.

Linear glacial erosion with constriction

The next series of simulations replicate glacial flow through a constriction in the valley width. The constriction is positioned at the halfway point of the model glacier, as in the perturbation simulation, and simulated by imposing a friction factor of 0.5 on the ice sliding rule. The maximum friction value is again tapered by using a sinc function. Final profiles exhibit a steepened area centered at the midpoint of the valley (Figure 13). The constriction impedes ice flow, causing the ice height to increase just upvalley from the midpoint (Figure: 14). Because sliding velocity, and consequently sub-glacial erosion, is a function of ice surface gradient, this increase in ice height causes the ice surface gradient to increase through the constriction. The resulting increase in sliding velocity enhances erosion in the center of the valley, forming a steepened section in the profile immediately down valley of the location of the constriction. The ice height and valley profile eventually reach equilibrium and the topography of the valley floor stabilizes. Although a steepened portion of the valley develops, no overdeepening, riegel or steep headwall is formed.

Constriction with threshold slope for quarrying

Because existing glacial erosion rules tend to smooth perturbations, I experimented with modifying these rules so as to produce a distribution of erosion that match my field observations. Specifically, I observe that the downstream sides of riegel are intensively plucked, whereas erosion in other areas is dominated by abrasion. One mechanism to produce such a distribution of erosion is to introduce a threshold slope for the onset of

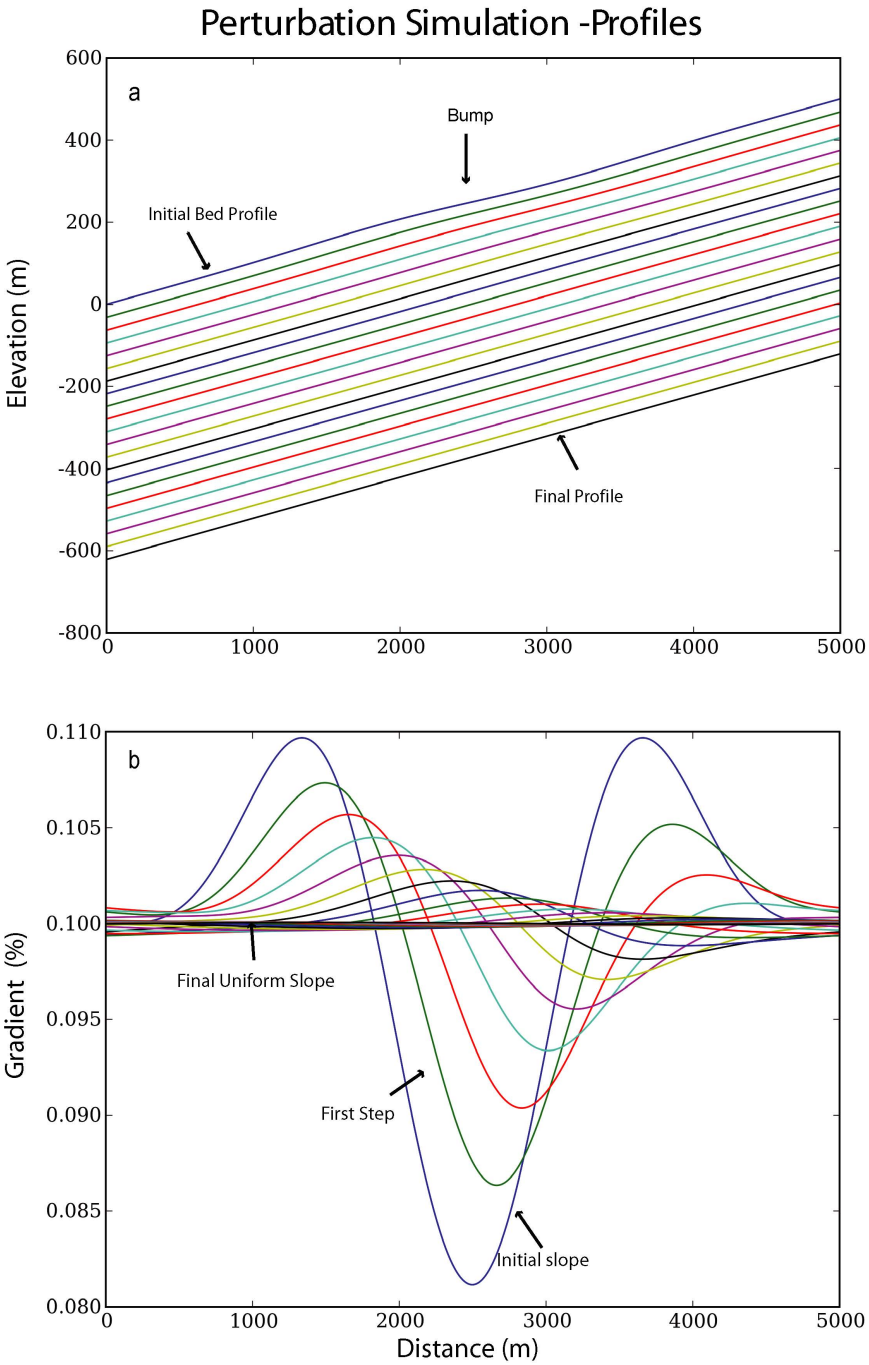

Figure 12
(a) Initial perturbation is smoothed away by abrasion and quarrying. (b) Graph of slopes. Initial slopes are quickly leveled and become uniform at the end of the simulation.

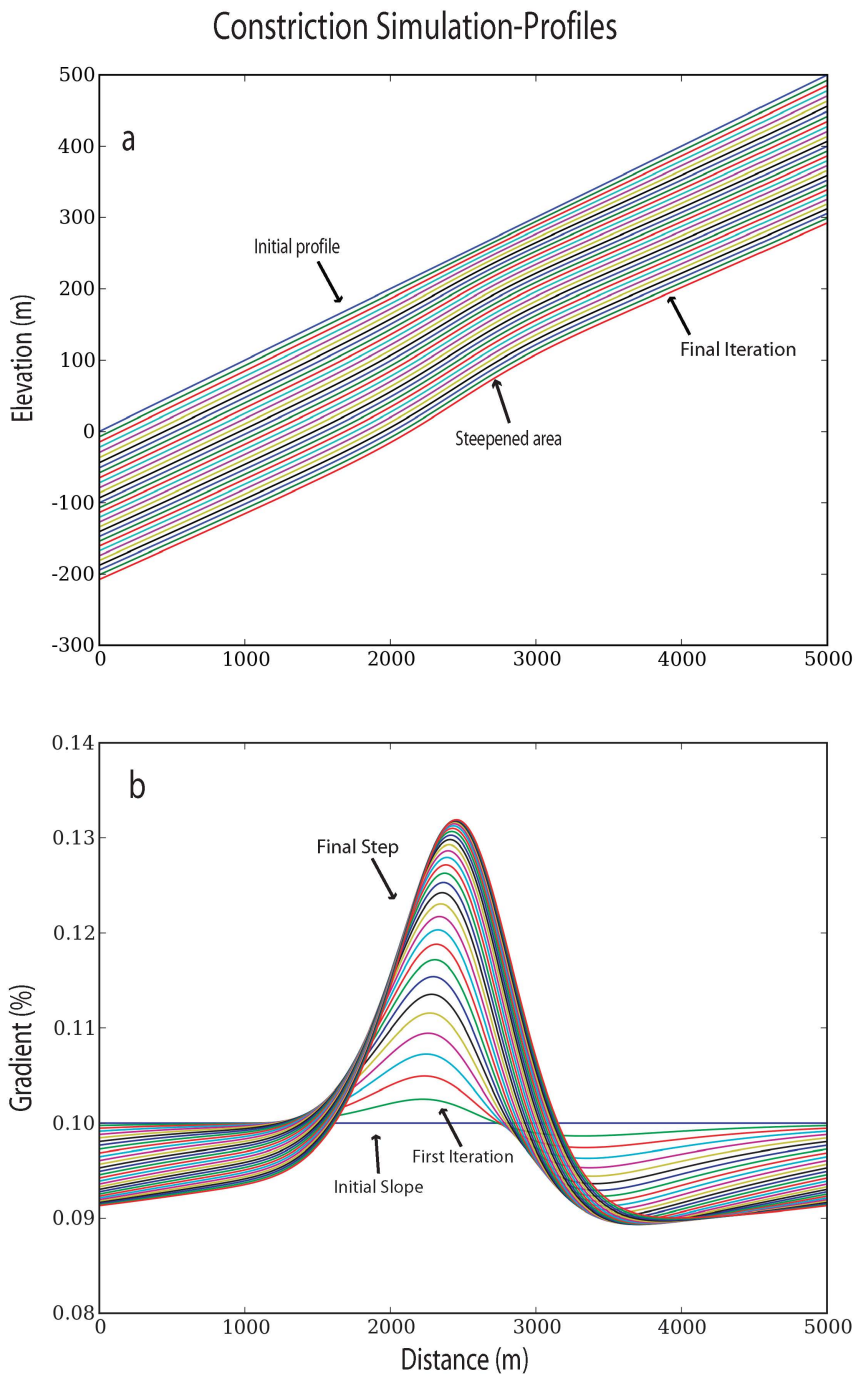

Figure 13
Constriction simulation. (a) Initial profile is flat and steepens just downvalley of location of maximum constriction. (b) Bed gradient gradually increases in center of valley at the location of maximum constriction due to increased erosion through constricted area. Gradient reaches stable state at end of simulation.

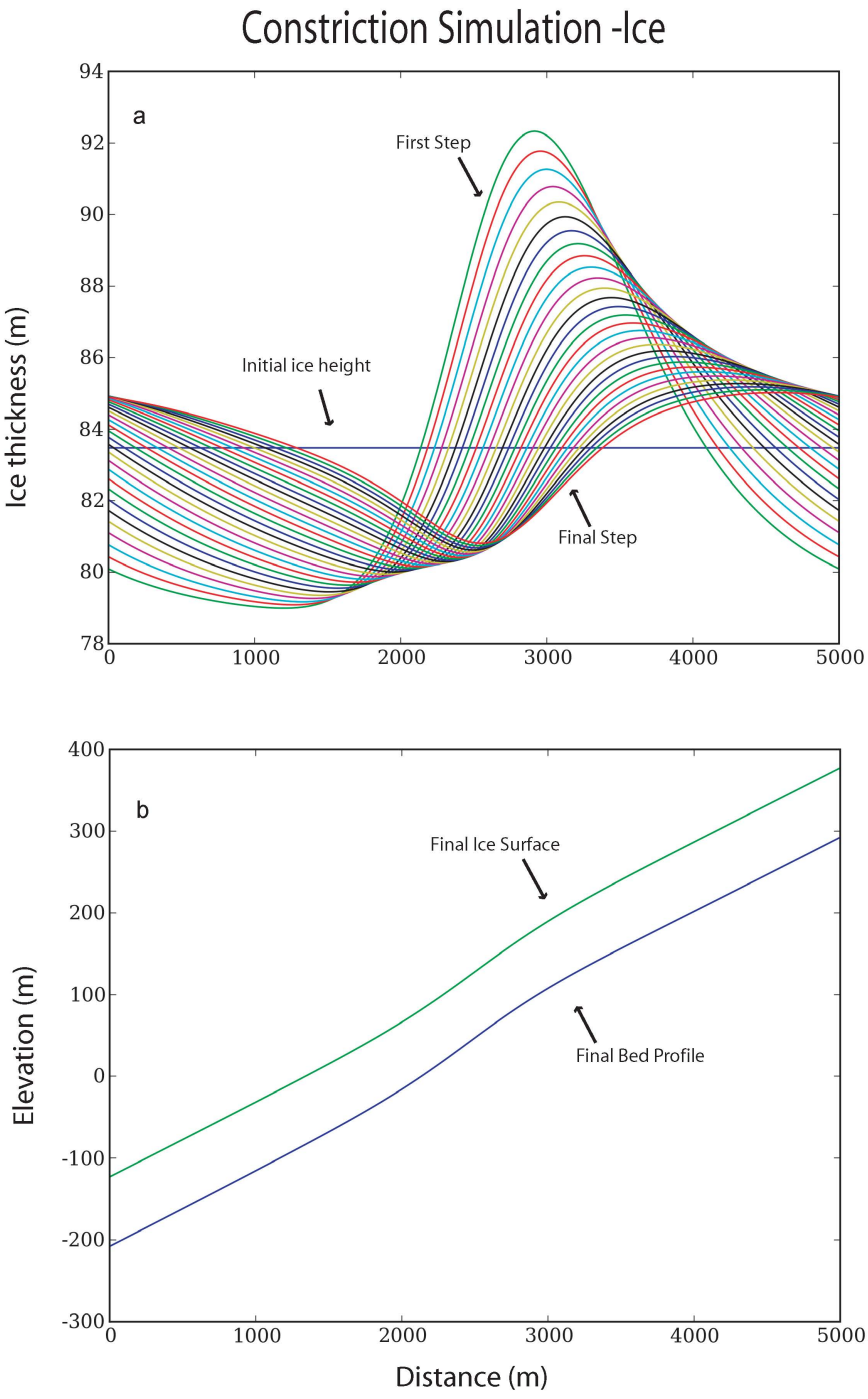

Figure 14
(a) Ice piles up behind constriction,thus increasing the sliding velocity and erosion through the constricted area. (b) The final profiles show a steepened area at the location of the constriction; ice and bed profiles are stable.

erosion by plucking. Changing erosion rules in this manner provided interesting results. The same friction factor of 0.5 was used to constrict the valley as in the former constriction simulation. However, in the following simulations, quarrying commences only after the bed profile steepens and reaches a threshold slope of 12.5 %. In all simulations, enhanced quarrying at the steepened valley section creates steps that propagate upvalley.

The initial simulation (Figure 15) has an abrasion constant that is much less than the quarrying constant ($C_{ab} = 0.0002$; $C_{qu} = 0.0009$). The average ice height between each node is used to calculate the sliding velocity, as this is a function of the ice surface gradient. The enhanced sliding velocity through the constricted section causes a steepened area to erode in the center of the model valley, and quarrying commences at model step 13, when the threshold slope of 12.5% is attained. Then the model glacier preferentially erodes at the steepened part and thus greater erosion occurs upvalley from the location of the constriction. An overdeepening forms in step 14 and expands through step 15, until the model becomes unstable due to the uneven ice surface.

In the next model simulation, the erosion constants remain the same, but the model calculates the sliding velocity from an effective ice height averaged over a larger area than between adjacent nodes (Figure 16). This is a more realistic approximation of glacier flow when the ice height is significantly greater than the node spacing. As in previous simulations, erosion by quarrying initiates after the middle section is steepened beyond the threshold gradient. A slight overdeepening forms at the steepened area in the center of the valley profile at model step 7 and retreats as a kinematic wave. As these overdeepenings develop they exhibit a slight increase in concavity. The floor gradually lengthens and smoothes as the

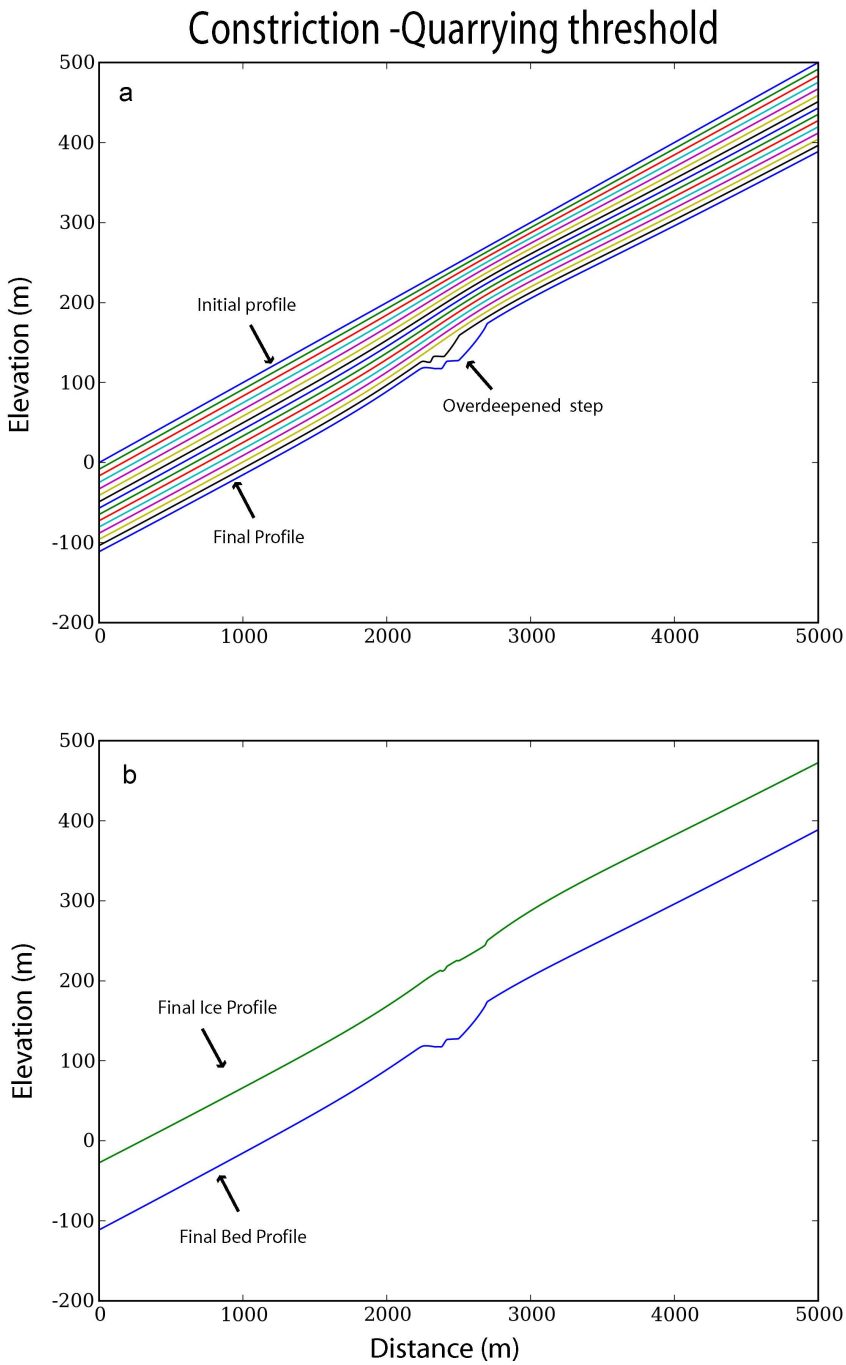

Figure 15
(a) Ice thickness from adjacent nodes was used to calculate surface gradient, and thus sliding velocity and erosion. Cab =0.0002; Cqu = 0.0009. Large overdeepening forms after 12.5% threshold gradient is crossed, and begins to propagate back. Instability reached after two quarrying steps. (b) Final profile is overdeepened and final ice surface is uneven.

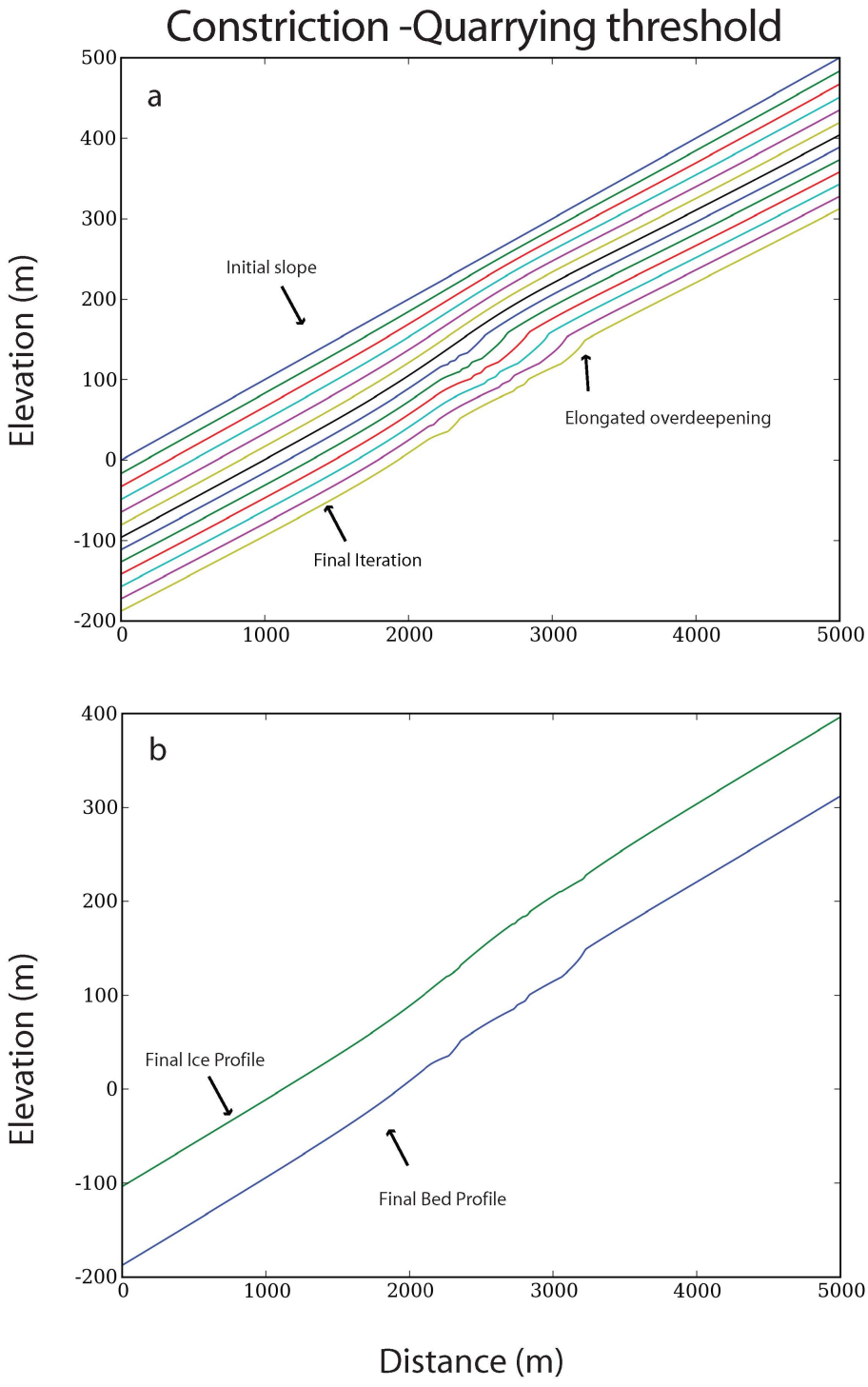

Figure 16
Constriction simulation with threshold gradient of 12.5%. Effective ice height is used to calculate ice motion and erosion. Cab = 0.0002, Cqu = 0.0009. Gentle overdeepening forms and propagates up valley. Shape of overdeepening is elongated until the model becomes unstable from uneven ice surface at step 12.

headwall retreats during each erosion step until the model becomes unstable at model step 11.

The next model run highlights the role of the erosion constants in the valley geometry (Figure 17). The effective ice height is used to calculate sliding velocity, with equivalent abrasion and quarrying coefficients (C_{ab} = 0.0001; C_{qu} = 0.0001). A step is eroded at the steepened section, as in previous simulations; however, the shape of the quarried region is preserved and the slope of the step "headwall" remains uniform through subsequent iterations. Steps systematically erode upvalley, removing a constant amount of quarried material during each iteration.

To test the validity of the chosen erosion coefficients, simulations were run in which the values of C_{ab} and C_{qu} are within range of measured erosion rates (Figure 18). These coefficients are less by an order of magnitude (C_{ab} = 0.00002; C_{qu} 0.00009). A much smaller amount of material is removed than in previous simulations where C_{ab} and C_{qu} were relatively large numbers. Some steps are formed and begin to propagate upvalley, but no more than ~500-1000 meters from the constriction before they are smoothed away. The corners of the steps appear to be smoothed by numerical diffusion over the order of magnitude greater time steps required for this model. This lowers the bed gradient below the quarrying threshold and leads to leveling of the steps.

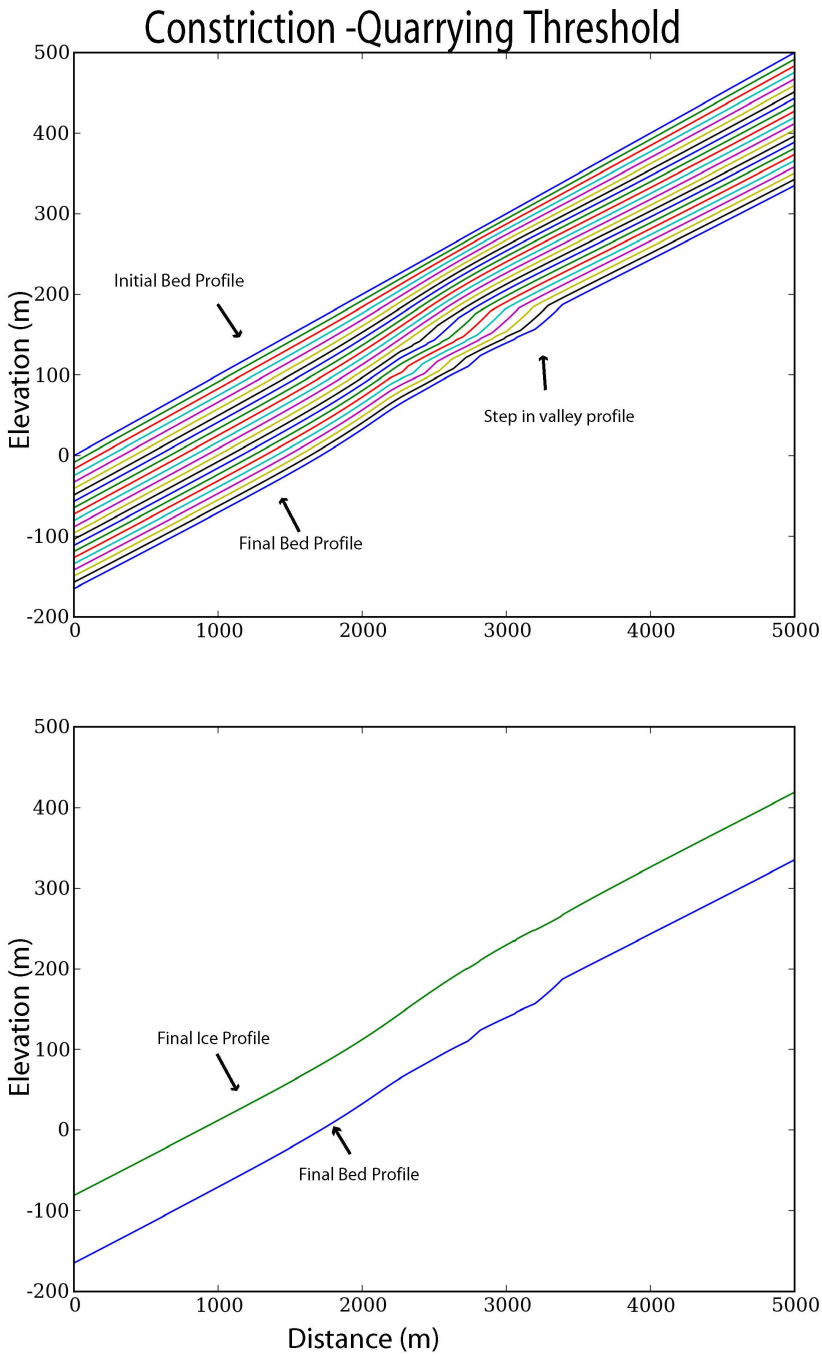

Figure 17

Constricted valley with threshold quarrying gradient of 12.5%. Cab = Cqu =0.0001

Eroded steps propagate from area of maximum constriction; step shape remains constant and slope of headwall remains uniform. No distinct overdeepening is formed.

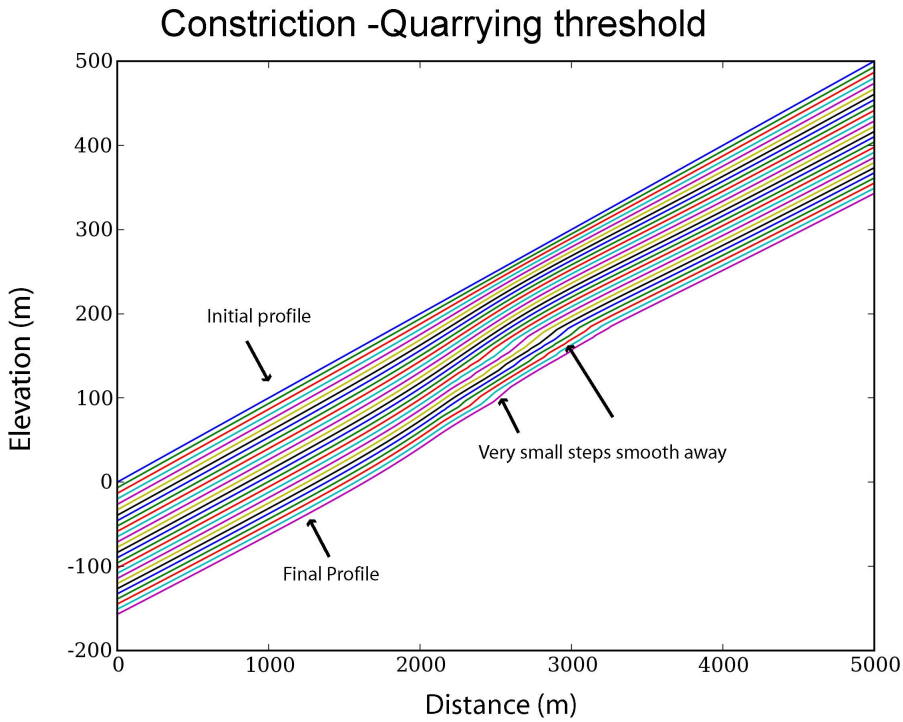

Figure 18
Constriction simulation with threshold quarrying run with very small abrasion and quarrying coefficients. Cab = 0.00002; Cqu = 0.00009 Some steps form and begin to propagate back, but are smoothed away after several iterations. For clarity, valley elevation profiles were recorded after every 4000 years of erosion.

Discussion

Cirque morphometry

Because valleys located at higher altitudes are able to sustain glaciers for longer periods of time, the cirques at higher elevations should have undergone more cycles of glaciation than cirques with comparable latitude and aspect at lower elevations. As Hengst Ridge is an area where aspect, general meso-climate, and catchment areas are comparable, and elevation is the main variant, it is plausible to assume that Tar Gap, which is the most westerly and is located at the lowest elevation, has been glaciated less than East or West Mineral Lakes cirques, and the Mosquito Lake cirque has undergone more cycles of glaciation for longer time periods. This progression of cirques thus permits a space-for-time substitution, whereby more easterly, higher-elevation cirques have undergone more frequent and longer glaciations than westerly, lower-elevation cirques. In the following discussion the four cirques that ornament Hengst Ridge are interpreted to represent a succession in development from Tar Gap in the west to Mosquito Lake in the east, corresponding to different stages in cirque formation.

Morphometric parameters measured in the study area do indicate that riegel form in stages, similar to those outlined in the hypothesis. The height of the cirque lip and degree of overdeepening both increase with elevation, from Tar Gap to Mosquito Lake. Tar Gap has no measurable riegel, and the valley profile slopes gently downvalley with no overdeepening. The Mineral Lakes cirques have only bedrock shoulders on the sides of the cirque lip, and

lack a defined valley-spanning bedrock ridge. Mosquito Lake cirque has a well-defined transverse bedrock ridge and a lake-filled overdeepening. Though these observations support the contention that riegel initially form as shoulders and expand inward from the sides, the observations do not explicitly support that fluctuating levels of ice occupation in a glacial valley lead to the formation and expansion of cirques. These observations do, however, support that perturbations in the glacial valley floor grow over time – a pattern further explored in the numerical modeling part of this study.

The trends in cirque development at Hengst Ridge agree in general with previous studies that have examined spatial variations in cirque morphometry to understand the processes of glacial landscape formation through time (e.g. Sugden, 1969; Trenhaile, 1974; Gordon, 1977; Evans and Cox, 1995; Garcia-Ruiz et al., 2000; Gordon, 2001; Brooke et al., 2006). Larger cirques have often been interpreted to be better developed (Olyphant, 1981; Sugden, 1977), with a greater concavity in both plan and profile closure than less mature cirques (Evans and Cox, 1995). Much of the observed increase in cirque size with time is due to increased length more than width or depth, so the larger size or greater area of well-developed cirques can be attributed to headwall backwearing. For example, by characterizing the morphometry of cirques in the Spanish Pyrenees, Garcia-Ruiz et al. (2000) found statistical correlations between altitude and two of the measured indices: cirque length (or specifically the length to width ratio), and amount of overdeepening. They found that the length to width ratio is much less than one at lower elevations, and much closer to or greater than one at higher elevations. Among the studies that employed space-for-time substitution, only Brooke et al. (2006) had sufficient climatic and uplift-rate data to deduce the time of glacial occupation in the field area. Their results agreed with the findings of Garcia-Ruiz et al. (2000), in which both length

of cirque and degree of overdeepening increased with ice occupation. Likewise, the results of this analysis of the Hengst Ridge cirques also indicate that both the length and degree of concavity (both plan and profile closure) increase as time of glacial occupation increases.

The observation that cirque length increases more than width or depth provides further evidence that locally enhanced erosion at the base of cirques probably drives headwall backwearing (e.g. Brocklehurst and Whipple, 2002; Oskin and Burbank, 2005; Naylor and Gabet, 2007). Other explanations for headwall retreat, such as mass wasting at the headwall due to frost shattering from temperature fluctuations, would operate in all directions away from the cirque floor and not give rise to the observed valley lengthening. Because the cirques are lengthened more than widened, and because greater overdeepening is also correlated with altitude in the Hengst Ridge study area, it is clear that processes that are at work in a cirque at the base of a glacier are responsible for cirque retreat. Thus, it is useful to look at the record of ice flow patterns preserved in the cirques to evaluate more closely the mechanisms with which cirques and their associated riegel form.

Ice Flow

Moving averages of striae trends show modest convergence of ice flow in the vicinity of riegel. These areas also show localized variation of ice-flow direction near the valley axis (Figure 19). Despite the evidence for convergent flow, little evidence was found for progressive focusing of ice flow into the center of the riegel with decreasing ice occupation. Rather the striae record a single, continuously varying pattern of ice flow across the riegel.

The overall patterns of ice-flow convergence follow the progressive development of cirque form along Hengst Ridge. Overall ice-flow convergence was evident in the Mosquito Lake cirque and the East Mineral Lake cirque, but the West Mineral Lake cirque exhibited

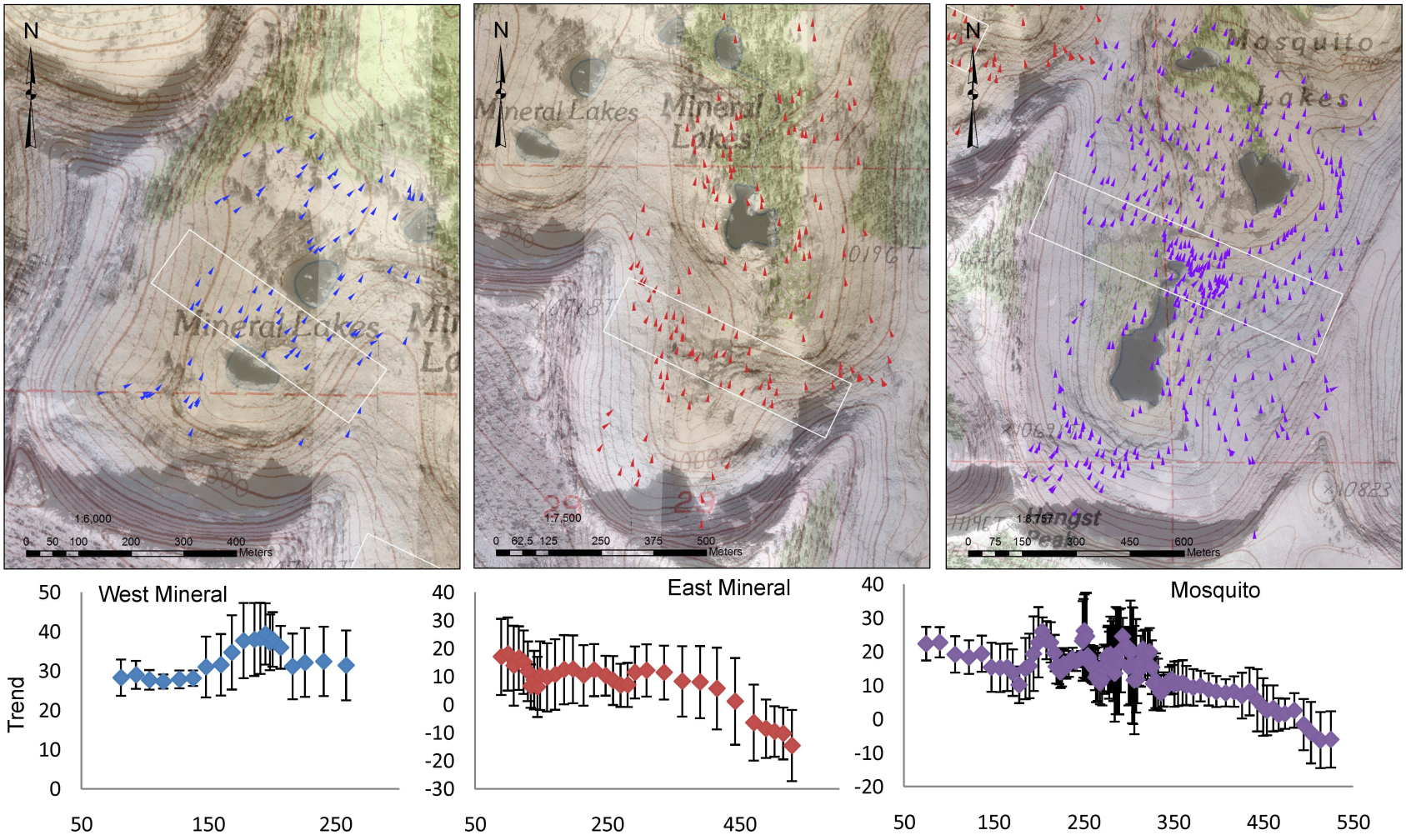

Figure 19
Striae orientations collected at the riegel of each cirque were plotted as a function of distance along transect, with the origin at the westernmost edge. A moving average of seven data points was used to smooth out local variations and hightlight overall trends in flow direction. W Mineral trends are relatively uniform and diverge slightly; E Mineral trends converge overall; Mosquito trends converge overall with enhanced variablilty near the cirque axis. White boxes highlight selected data.

slight divergence. Flow patterns in the Mosquito Lake cirque are more variable than either of the Mineral Lakes cirques, with much of the variability localized lower in the cirque near the valley axis. The East and West Mineral Lake cirques exhibit relatively uniform trends across the riegel. In all cases no clear evidence of stronger ice-flow convergence during waning stages of glaciation was found. What convergence does exist is likely to be the result of lateral flow of ice towards areas of faster-moving ice in the valley axis (Harbor et al., 1997)

From reconstruction of ice thickness, the heights of the glaciers that occupied the Mineral Lakes and Mosquito Lakes valleys varied by a factor of two. The maximum thickness increased from ~90m in the West Mineral Lake cirque to ~110m in the East Mineral Lake cirque, and ~180m in the Mosquito Lake cirque. Because the effective viscosity of ice varies exponentially with deviatoric stress, and thus ice thickness, ice may have flowed much more readily around local bed topography underneath the thickest part of the glacier. This would provide a plausible explanation for the variability of striae orientations observed near the center of valleys. Because one of the factors affecting the effective viscosity of ice is its deviatoric stress, which is higher at greater depths, a unit of ice at depth in a glacier will exhibit a higher strain rate and flow more fluidly than shallow ice.

A threshold in ice-flow behavior may help to further explain the differences in flow-field complexity over riegel at Hengst Ridge. By comparing measurements of deformation in multiple tilted boreholes in a block of the Worthington Glacier, Alaska to computed deviatoric stress values, Marshall et al. (2002), found that there exists a threshold ice thickness of ~115m, above which ice exhibits a linear viscous rheology (stress exponent = 1), and below which ice exhibits a non-linear rheology (stress exponent = 3 to 4). The trim line isopach maps establish that the ice in the last glacier to occupy the Mosquito Lake Cirque

was well above the ~115m threshold; East Mineral Lake was within error of the threshold, and West Mineral Lake was below the threshold thickness (Figure 20). This may account for the variability of striae trends found in the Mosquito Lake cirque and the relative lack of variation in the Mineral Lakes cirques. Mosquito Lake had highly variable flow vectors underneath the thickest ice. The lack of variability on the riegel of the Mineral Lakes is well explained by the thin ice occupying these particular cirques.

Striation orientations do not support the hypothesis that riegel form from fluctuating levels of ice occupation. In fact, the ice flow record that is preserved in the Hengst Ridge cirques neither substantiates nor invalidates this hypothesis. Instead, the striae orientations best support that the ice at depth flowed more fluidly in the center of the valley where ice thickness was greatest. The effect of this ice-flow threshold on erosion rates at the base of the glacier is not known. However, enhanced ice flow at the valley axis could promote enhanced erosion there, which would in turn help to develop a localized trough and constriction at the valley axis.

Numerical Model

Numerical simulations show that glacial abrasion and quarrying erosion-rate laws formulated similar to this tend to smooth subglacial topography. Only by introducing a threshold for quarrying could steps and overdeepenings be created in a valley without intersecting glaciers (e.g. MacGregor et al., 2000). These simulations explore the two processes and show how knowledge of the relative efficacy of abrasion and quarrying is important in determining glacial valley morphology, and how using extreme rules for erosion may be necessary to reproduce glacial valley topography.

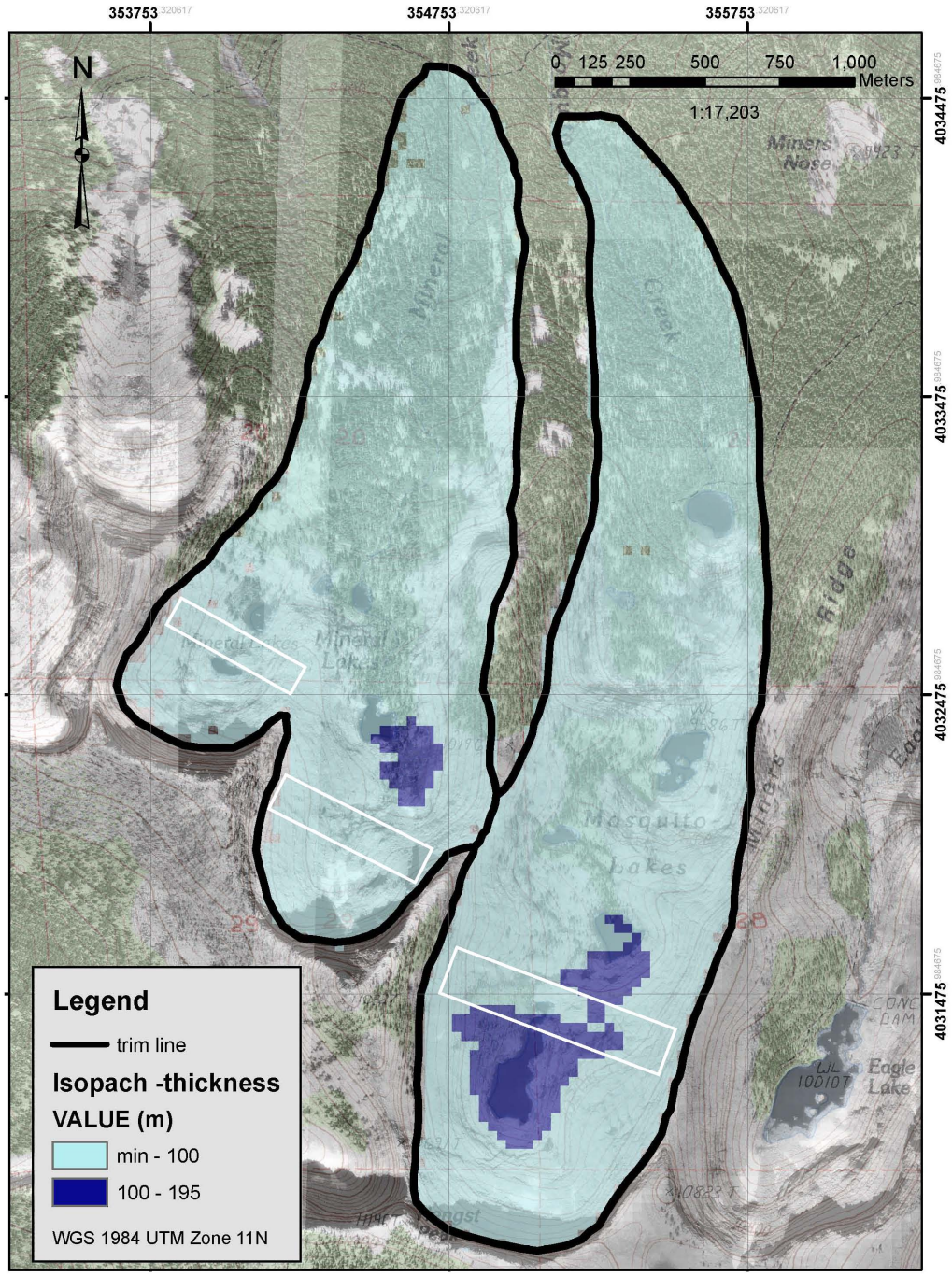

Figure 20
Thickness map of East and West Mineral Lakes and Mosquito Lakes cirques. Light blue denotes thickness less than 100m; dark blue highlights thickness greater than 100m. White boxes outline locations where trend data was extracted for trend plots.

In all simulations with an initial perturbation, the perturbation is smoothed away, showing that subglacial topography is reduced rather than enhanced by ice flowing over a bedrock ridge. It is important to note however that the ice-flow and erosion rules employed in this study are simplified. Crevasse formation is likely just downvalley of a transverse perturbation due to the tensile stresses induced above at the ice surface (Hooke, 1991). The subsequent melt water input at these crevasses may locally enhance subglacial quarrying (Iverson, 1991; Cohen et al., 2006), which should accentuate relief. The migration of meltwater and crevasse formation was not modeled in this study, and thus it remains uncertain whether a perturbation alone could give rise to an overdeepening.

In simulations containing a persistent valley constriction, an overdeepening could be produced only when a threshold for quarrying is included. Without such a threshold locally steepened slopes are eroded just downvalley of the location of maximum constriction. With a quarrying threshold a step may be formed once the threshold is crossed (Figure 15). This steep step begins to move upvalley as a kinematic wave before the instability of the model causes it to crash. Although the instability limits this analysis, it is plausible to postulate that the gently sloping floor would have begun to lower via abrasion and the steepened headwall would move back from enhanced quarrying. The final result would likely have been an elongated overdeepening, which correlates well with the lengthened profile that has been suggested for mature cirques by this morphometric study and others (e.g. Evans and Cox, 1995; Garcia-Ruiz et al., 2000; Evans, 2006).

In their numerical modeling study of headwall processes, MacGregor et al. (2009) included additional terms addressing the input of windblown snow and the reduction of erosion due to sediment cover. However no threshold gradient for quarrying was applied in

their simulations. Quarrying was driven nonlinearly by the product of sliding velocity and the sine of the bed slope. Similar to the model presented here, theirs is a heuristic rule, based on observations of enhanced quarrying on lee sides of glacial erosional features such as riegel and rouche moutonees. Only rules that did not produce extreme topographic features were used, so if topography was produced anywhere in the model valley it was considered very likely to form in nature. This continuously varying quarrying rule avoids the instability that arises in the model presented here. Yet the model by MacGregor et al. (2009) cannot give rise to abrupt steps in glacial valley profiles.

In the model presented here, steepening occurs at the location of the constriction, but no overdeepening occurs until the threshold slope for quarrying is crossed. This indicates that the erosion rule needs to include a term representing a threshold bed slope, above which quarrying is the dominant erosive process, and below which abrasion is dominant. Introducing a threshold slope for quarrying, although extreme, appears necessary to form steps and overdeepenings in glacial valleys, and calibration to actual glacial valley geometries would be a useful endeavor.

Relative efficacy of abrasion and quarrying

In addition to emphasizing the value of including a threshold slope for quarrying, this model indicates that (1) the relative efficacy of abrasion and quarrying, or the ratio of erosion coefficients, are important in determining the presence, shape, and magnitude of overdeepenings and step headwalls, and (2) quarrying is more efficient at removing material than abrasion. The degree of overdeepening and shape of the step and headwall changes depending on the ratio of erosion coefficients chosen for each simulation. Where the chosen coefficient of quarrying was much greater than the coefficient of abrasion, the headwall

forms were more curved with more elongated overdeepenings than simulations where abrasion and quarrying coefficients were equal. In a simulation where the values of abrasion is much less than quarrying (Figure 16), an overdeepening forms and is lengthened after each iteration, whereas simulations with equivalent abrasion and quarrying values fail to produce an overdeepening and have a step with a constant linear slope throughout each model step (Figure 17).

Because glacial valleys are characterized by steps and overdeepenings, and some studies indicate that the maximum headwall gradient and length increase with cirque maturity (Evans and Cox, 1995; Garcia-Ruiz et al., 2000; Evans, 2006), the simulations in which quarrying is a more dominant erosive process than abrasion are more realistic. Thus, in modeling valley erosion, the coefficient of quarrying should be greater than the coefficient of abrasion. This agrees with field observations of sediment evacuation by glaciers, which suggest that quarrying is much more efficient a process than abrasion (e.g. Boulton et al., 1979; Hallet et al., 1996; Briner and Swanson, 1998). Moreover, because the specific values of realistic coefficients are unknown, it would be useful for further studies to test this and calibrate to actual field measurements.

Magnitude of erosion coefficients

In previous simulations of headwall erosion, MacGregor et al. (2009) showed that the magnitude of erosion was a direct reflection of the value of the erosion coefficients. However, final valley forms were not greatly affected by the values or ratios of coefficients. The erosion constants utilized by these authors were within range of field measurements of the relative efficacy of abrasion and quarrying (e.g. Hallet et al., 1996) and the ratio of abrasion to quarrying was based on observations of the Variegated Glacier during a surge

(Humphrey and Raymond, 1994). Their model showed greater quarrying at the valley head, which is a direct result of the steeper gradient found there, and greater abrasion where ice was thickest. Alternative erosion coefficient pairings were tested, but the final profiles were similar. This led to the postulation that different erosion-rule coefficients would not produce very different valley profiles; a statement that contradicts the results presented here.

My model simulations show that the form of the profile change according the ratio of coefficients chosen. Where abrasion and quarrying are equal, the step profiles are very linear, compared to simulations where abrasion is greater than quarrying. These steps have curved, elongated profiles. Therefore, simulations that include a threshold slope for quarrying indicate that the final valley profiles are in fact sensitive to the ratio of erosion-rate coefficients, and that it would be useful to test different pairings and calibrate these with field observations of the relative rates of abrasion and quarrying beneath active glaciers.

The magnitude of erosion coefficients may also be important in determining the valley profile geometry, but the modeling scheme used here may be too simple to accurately model the formation of overdeepenings. In simulations with relatively small coefficients the very slight overdeepening that begins to form is smoothed away after a few iterations (Figure 18). In simulations where the coefficients are larger by an order of magnitude (Figure 15, 16, 17), overdeepenings form and headwalls retreat, although these simulations reach an unstable state. Simulations with smaller coefficients have smaller erosion steps and produce a more stable model, yet greater inaccuracy may be introduced in the form of numerical diffusion, which is an inherent limitation in finite-difference numerical modeling (Peterson, 1992). Other modeling approaches appear necessary to further explore the formation and retreat of overdeepenings.

Conclusions

This thesis describes an attempt to understand the formation of riegel and ultimately the mechanisms that cause cirque retreat. Using space-for-time substitution to analyze the morphometric characteristics measured in the field portion of this study indicate that existing perturbations may tend to grow through time, and thus lend support to the hypothesis that fluctuating levels of glacial occupation in a valley leads to the development of cirques. Additionally, it is indicated that mature cirques are slightly elongated, with flattened valley floors and steep headwalls. If mass wasting at the headwall is the process solely responsible for cirque retreat, then cirques would be expected to expand outward equally in all directions. So it is implied that the processes of erosion at the base of a glacier near the headwall are responsible for cirque retreat.

Analyzing the most recent ice flow patterns from striation orientations preserved in the cirques show that flow converges along the riegel of mature cirques and flows more uniformly, with slight divergence, in cirques interpreted to be younger. Highly variable flow directions at the axis of the Mosquito Lake cirque are most likely linked to fluid flow beneath deep ice. The data supports assertions by Marshall et al. (2002) that a threshold depth exists, above which the strain rate of ice increases linearly with depth and below which the strain rate increases exponentially. This fluidly flowing ice could in turn lead to enhanced erosion along the cirque axis, where ice is thicker, and thus lead to the formation of bedrock shoulders.

Numerical model simulations indicate that ice smoothes away any initial perturbation. However, it is generally accepted that bedrock perturbations lead to crevasse formation at the surface and the subsequent water input causes quarrying that leads to amplified bedrock topography (Hooke, 1991). It is possible that flow over a perturbation is too complex to be accurately modeled by the simplified erosion and ice flow dynamics in the numerical model presented here. Meltwater and crevasse formation were not addressed in this model, so it remains inconclusive whether perturbations lead to enhanced quarrying and increased topographic relief.

However, simulations of ice flow through bedrock shoulders do show that the build-up of ice behind the constriction leads to steeper surface slopes, enhanced erosion, and steepening of the bed through the constriction. Steps and overdeepenings are produced when a quarrying threshold is applied. Although more parameters lead to increased quarrying than simply the gradient of the bed below a glacier (e.g. the relative hardness of the bedrock, location of existing joints, crevasses at the surface, length of cavities between ice and bedrock), the modeling results provide a strong argument that a quarrying threshold is necessary to create the characteristic glacial valley topography. It would be valuable for future modeling attempts to test different quarrying thresholds and calibrate them to field observations. This study also indicates that the relative efficacy of abrasion and quarrying are very important when a quarrying threshold is used to model erosion, and it would be useful to test different ratios and magnitudes of erosion, and closely calibrate them to actual rates of erosion from field studies.

Appendix
Model Code

```
import math, cPickle
from pylab import *
#
# Constants
#
gravity = 9.81
rho_ice = 917
rho_water = 1000
F          = 1
C1         = 0.0012
C2         = 0.0001
C3         = 0.00025
C4         = 0.00095
A          = 2.1e-16
J          = A * 2 / 5 * (F * F * F) * (rho_ice * rho_ice * rho_ice) * (gravity * gravity * gravity)
K          = C1 * F * rho_ice * gravity

class Profile:

   def __init__(self,length,dx,slope):
      self.z = array(range(0,length,dx),typecode = Float64)
      self.number_of_elements = len(self.z)
      self.z = self.z * slope
      self.dx = dx
      self.length = length
      self.slope = slope
      self.friction = ones((self.number_of_elements), typecode = Float64)

   def perturb(self,amplitude):
      perturbation_base  = array(range(0,self.length,self.dx), typecode = Float64)
      perturbation  = sin(perturbation_base * 2 * pi / self.length) * amplitude
      sync_function = (sin(perturbation_base * pi / self.length) *
                  sin(perturbation_base * pi / self.length) *
                  sin(perturbation_base * pi / self.length) *
                  sin(perturbation_base * pi / self.length))

      self.z = self.z + perturbation * sync_function

   def perturbFriction(self,minimum_friction):
         perturbation_base  = array(range(0,self.length,self.dx), typecode = Float64)
      perturbation  = ((1 - cos(perturbation_base * 2 * pi / self.length)) / 2 ) * (1 - minimum_friction)
      sync_function = (sin(perturbation_base * pi / self.length) *
                  sin(perturbation_base * pi / self.length) *
                  sin(perturbation_base * pi / self.length) *
                  sin(perturbation_base * pi / self.length) *
```

```
                sin(perturbation_base * pi / self.length) *
                sin(perturbation_base * pi / self.length) *
                sin(perturbation_base * pi / self.length) *
                sin(perturbation_base * pi / self.length))


        self.friction = self.friction - perturbation * sync_function

    def gradient(self):
                return (concatenate((self.z[1:],self.z[:1])) - concatenate((self.z[-1:],self.z[:-1]))) / (2 *
self.dx)


class IceProfile:

        def __init__(self,profile,flux):
                self.profile = profile
                self.flux = flux
                self.number_of_elements = profile.number_of_elements
                self.length = profile.length
                self.dx = profile.dx
                S = profile.slope

                H = 0
                intervals = [1,.1,.01,.001]
                for i in intervals:
                        while 1:
                                H = H + i
                                testflux = (K * H * H * S * S) + (J * S * S * S * H * H * H * H * H)
                                if testflux > flux:
                                        H = H - i
                                        break
                self.initial_ice = H
                self.initial_sliding     = - K * H * S * abs(S)
                self.initial_deformation = - J * H * H * H * H * S * S * S
                self.resetIce()

        def resetIce(self):
                self.ice = ones((self.number_of_elements), typecode = Float64)
                self.ice = self.ice * self.initial_ice

        def iceGradient(self):
                gradient = (diff(self.profile.z) + diff(self.ice)) / self.dx
                gradientbegin = ((self.profile.z[0] + self.ice[0]) - (self.profile.z[-1] + self.ice[-1]) +
                                                (self.profile.slope * self.profile.length)) / self.dx

                return concatenate(([gradientbegin],gradient))
```

```
def resetFloorGradient(self):

        rise = self.profile.slope * self.profile.length
        end2 = self.profile.z[0] + rise
        end3 = self.profile.z[1] + rise
        begin1 = self.profile.z[-1] - rise
        begin2 = self.profile.z[-2] - rise
        begin3 = self.profile.z[-3] - rise

        f1 = self.profile.z
        f2 = concatenate((self.profile.z[1:],[end2]))
        f3 = concatenate((self.profile.z[2:],[end2,end3]))
        b1 = concatenate(([begin1],self.profile.z[:-1]))
        b2 = concatenate(([begin2, begin1],self.profile.z[:-2]))
        b3 = concatenate(([begin3, begin2, begin1],self.profile.z[:-3]))

        w1 = 1
        w2 = 1
        w3 = 1

        s1 = (f1 - b1) / self.dx
        s2 = (f2 - b2) / 3 / self.dx
        s3 = (f3 - b3) / 5 / self.dx

        self.floor_gradient = ( s1 * w1 + s2 * w2 + s3 * w3 ) / ( w1 + w2 + w3 )


def smoothProfile(self):

        rise = self.profile.slope * self.profile.length
        end1 = self.profile.z[0] + rise
        end2 = self.profile.z[1] + rise
        begin1 = self.profile.z[-1] - rise
        begin2 = self.profile.z[-2] - rise

        z0 = self.profile.z
        f1 = concatenate((self.profile.z[1:],[end1]))
        f2 = concatenate((self.profile.z[2:],[end1,end2]))
        b1 = concatenate(([begin1],self.profile.z[:-1]))
        b2 = concatenate(([begin2, begin1],self.profile.z[:-2]))

        w0 = 1
        w1 = 1
        w2 = 0

        self.profile.z = (z0*w0 + f1*w1 + b1*w1 + f2*w2 + b2*w2) / (w0 + w1 + w1 + w2 + w2)
```

```
	def floorGradient(self):
		return self.floor_gradient

	def iceHeight(self):
		return (concatenate((self.ice[1:],self.ice[:1])) + self.ice) / 2

	def effectiveHeight(self):
		H = self.iceHeight()
		L = len(H)
		effective_ice = ones(L, typecode = Float64)
		totalH = concatenate((H,H,H))
		for x in range(0,L):
			Q = totalH[ L + x - int(self.initial_ice / 2 / self.dx) : L + x + int(self.initial_ice / 2 /
self.dx)]
			effective_ice[x] = (sum(Q)/len(Q))
		return effective_ice

	def slidingVelocity(self):
		H = self.iceHeight()
		S = self.iceGradient()
		F = self.profile.friction
		sliding = - K * H * S * abs(S) * F
		return sliding

	def effectiveSlidingVelocity(self):
		H = self.effectiveHeight()
		S = self.iceGradient()
		F = self.profile.friction
		sliding = - K * H * S * abs(S) * F
		return sliding

	def deformationVelocity(self):
		H = self.iceHeight()
		S = self.iceGradient()
		F = self.profile.friction
		deformation = - J * H * H * H * H * S * S * S * F
		return deformation

	def slidingFlux(self):
		H = self.iceHeight()
		S = self.iceGradient()
		F = self.profile.friction
		sliding = - K * H * H * S * abs(S) * F
		return sliding


	def deformationFlux(self):
		H = self.iceHeight()
```

```
        S = self.iceGradient()
        F = self.profile.friction
        deformation = - J * H * H * H * H * H * S * S * S * F
        return deformation

def moveIce(self,flux,years):
        flux_out = concatenate((flux[1:],flux[:1]))
        self.ice = self.ice + (flux - flux_out) / self.dx * years

def erodeBed (self,years):
        sliding = self.effectiveSlidingVelocity()
        velocity = (concatenate((sliding[1:],sliding[:1])) + sliding) / 2

        threshold_slope1 = 0.125

        abrasionquarrytest = (self.floor_gradient > threshold_slope1) * 1
        abrasiontest = (abrasionquarrytest - 1) * -1


        self.profile.z = self.profile.z + abrasionquarrytest * ((C3 * velocity) + (C4 * velocity *
                        (self.floor_gradient / sqrt((self.floor_gradient * self.floor_gradient) +
                        1)))) * years
        self.profile.z = self.profile.z + abrasiontest * (C3 * velocity) * years

        self.smoothProfile()
        self.resetFloorGradient()

def modelYear(self,steps_per_year):
        sliding_time = steps_per_year / 10
        step_size    = 1.0 / steps_per_year
        print "summer"
        for step in range(0,sliding_time):
                for slidestep in range(0,10):
                        self.moveIce(self.slidingFlux(),step_size)
                self.moveIce(self.deformationFlux(),step_size)
        print "winter"
        for step in range(sliding_time,steps_per_year):
                self.moveIce(self.deformationFlux(),step_size)

def modelRun(self,steps_per_year,convergence = 0.1):
        year = 0
        print "start"
        while 1:
                print "loop"
                old_ice = self.ice
                for step in range(0,10):
                        year = year + 1
                        self.modelYear(steps_per_year)
```

```
                print "year ", year
            print max(old_ice - self.ice) - min(old_ice - self.ice)
            print "decade check"
            if (max(old_ice - self.ice) - min(old_ice - self.ice)) < convergence:
                break

    def modelRunSet(self,steps_per_year,iterations,erosion,convergence = 0.1):
        self.resetFloorGradient()
        for step in range(0,iterations):
            print "Iteration: ", step
            self.modelRun(steps_per_year,convergence)
            self.erodeBed(erosion)



class Model:
    def __init__(self,steps_per_year, iterations, erosion, convergence = 0.1):
        self.steps_per_year = steps_per_year
        self.iterations = iterations
        self.erosion = erosion
        self.convergence = convergence

    def initiate(self,name,profile_length, step_length, slope, ice_flux, perturbation,
minimum_friction):
        self.name = name
        self.savestep = -1
        valley_floor = Profile(profile_length,step_length,slope)
        valley_floor.perturb(perturbation)
        valley_floor.perturbFriction(minimum_friction)
        self.glacier = IceProfile(valley_floor,ice_flux)
        print self.glacier.initial_ice, self.glacier.initial_sliding, self.glacier.initial_deformation
        self.valleyprofile = []
        self.iceprofile = []
        self.save()

    def load(self,name,savestep):
        model_file = open(name+"_"+str(savestep)+".mod",'rb')
        self.glacier = cPickle.loads(model_file.read())
        model_file.close()
        data_file = open(name+"_"+str(savestep)+".pro",'rb')
        self.valleyprofile = cPickle.loads(data_file.read())
        data_file.close()
        data_file = open(name+"_"+str(savestep)+".ice",'rb')
        self.iceprofile = cPickle.loads(data_file.read())
        data_file.close()
        self.name = name
        self.savestep = savestep
```

```
	def save(self):
		self.savestep = self.savestep + 1
		self.valleyprofile.append(self.glacier.profile.z)
		self.iceprofile.append(self.glacier.ice)
		model_file = open(self.name+"_"+str(self.savestep)+".mod",'wb')
		model_file.write(cPickle.dumps(self.glacier))
		model_file.close()
		data_file = open(self.name+"_"+str(self.savestep)+".pro",'wb')
		data_file.write(cPickle.dumps(self.valleyprofile))
		data_file.close()
		data_file = open(self.name+"_"+str(self.savestep)+".ice",'wb')
		data_file.write(cPickle.dumps(self.iceprofile))
		data_file.close()

	def run(self,number = 1):
		for step in range(0,number):
			print "Model step", (self.savestep + 1)
			self.glacier.modelRunSet(self.steps_per_year, self.iterations, self.erosion,
self.convergence)
			self.save()

	def graphSlopes(self):
		xaxis = array(range(0, len(self.iceprofile[0]) - 1))
		for i in range(0,len(self.valleyprofile)):
			plot(xaxis * self.glacier.dx,diff(self.valleyprofile[i]) / self.glacier.dx)
		show()

	def graphProfiles(self):
		xaxis = array(range(0, len(self.iceprofile[0])))
		for i in range(0,len(self.valleyprofile)):
			plot(xaxis * self.glacier.dx,self.valleyprofile[i])
		show()

	def graphIce(self):
		xaxis = array(range(0, len(self.iceprofile[0])))
		for i in range(0,len(self.iceprofile)):
			plot(xaxis * self.glacier.dx,self.iceprofile[i])
		show()

	def graphIceSlope(self):
		xaxis = array(range(0, len(self.iceprofile[0]) - 1))
		for i in range(0,len(self.iceprofile)):
			plot(xaxis * self.glacier.dx,diff(self.iceprofile[i]) / self.glacier.dx)
		show()

	def graphIceProfile(self,step = -1):
		xaxis = array(range(0, len(self.iceprofile[0])))
		plot(xaxis * self.glacier.dx,self.valleyprofile[step])
```

```
                plot(xaxis * self.glacier.dx,self.valleyprofile[step] + self.iceprofile[step])
                show()

        def graphDoubleIceProfile(self,step = -1):
                xaxis = array(range(0, len(self.iceprofile[0]) * 2), typecode = Float64)
                rise = self.glacier.profile.slope * self.glacier.profile.length
                profile = concatenate((self.valleyprofile[step],self.valleyprofile[step] + rise))
                ice = concatenate((self.iceprofile[step],self.iceprofile[step]))
                plot(xaxis  * self.glacier.dx / 1000,profile)
                plot(xaxis  * self.glacier.dx / 1000,profile + ice)
                show()

        def graphPresentProfile(self):
                xaxis = range(0, len(self.iceprofile[0]))
                valley = self.glacier.profile.z
                ice = self.glacier.ice
                for i in xaxis:
                        if ice[i] > 1000: ice[i] = 1000
                        if ice[i] < -1000: ice[i] = -1000
                plot(xaxis,valley)
                plot(xaxis, valley + ice)
                show()


def initiateModel(profile_length, step_length, slope, perturbation, ice_flux):
        valley_floor = Profile(profile_length,step_length,slope)
        valley_floor.perturb(perturbation)
        model = IceProfile(valley_floor,ice_flux)
        print model.initial_ice, model.initial_sliding, model.initial_deformation
        profile = []
        profile.append(model.profile.z)
        return (model,profile)

def loadModel(filename):
        model_file = open(filename+".mod",'rb')
        model = cPickle.loads(model_file.read())
        model_file.close()
        data_file = open(filename+".pro",'rb')
        profile = cPickle.loads(data_file.read())
        data_file.close()
        return (model,profile)

def saveModel(model,profile,filename):
        model_file = open(filename+".mod",'wb')
        model_file.write(cPickle.dumps(model))
        model_file.close()
        data_file = open(filename+".pro",'wb')
        data_file.write(cPickle.dumps(profile))
```

```
        data_file.close()

def appendProfile(model,profile):
        profile.append(model.profile.z)

def graphAllProfiles(profile):
        xaxis = range(0,len(profile[0]))
        for i in range(0,len(profile)):
                plot(xaxis,profile[i])
        show()

def graphAllSlopes(profile):
        xaxis = range(0,len(profile[0]) - 1)
        for i in range(0,len(profile)):
                plot(xaxis,diff(profile[i]))
        show()

def goBack(model,profile,steps):
        model.profile.z = profile[- steps - 1]
        model.resetIce()
```

References

Alley, R. B., Strasser, J.C., Lawson, D.L., Evenson, E.B., Larson, G.J. (1999). "Glaciological and geological implications of basal-ice accretion in overdeepenings." Glacial Processes, Past and Present, Geological Society of America Special Paper 337. Geological Society of America: 1-9.

Alley, R. B., Lawson, D.E., Larson, G.J., Evenson, E.B., Baker, G.S. (2003). "Stabilizing feedbacks in glacier-bed erosion." Nature 424: 758-760.

Anderson, R. S., Molnar, P., Kessler, M.A. (2006). "Features of glacial valley profiles simply explained." Journal of Geophysical Research 111(F1).

Augustinus, P.C. (1992). "The influence of rock mass strength on glacial valley cross-profile morphometry; a case study from the Southern Alps, New Zealand." Earth Surface Processes and Landforms 17(1): 39-51

Bateman, P.C. and Eaton, J.P. (1967). "Sierra Nevada Batholith." Science 158(3807): 1407-1417

Bateman, P.C. (1969). "Geology of the Sierra Nevada: pts 1-2." Mineral Information Service 1(22): 39-42

Boulton, G.S. (1974). "Processes and patterns of glacial erosion." Glacial Geomorphology: proceedings

Briner J.P. and Swanson, T.W., (1998). "Using inherited cosmogenic 36Cl to constrain glacial erosion rates of the Cordilleran ice sheet." Geology 26: 3-6

Brocklehurst, S. and Whipple, K. X. (2002). "Glacial erosion and relief production in the Eastern Sierra Nevada, California." Geomorphology 42: 1-24.

Brocklehurst, S., Whipple, K.X., and Foster, D. (2004). "Ice thicknes and topographic relief in glaciated landscapes of the western USA." Geomorphology 97: 35-51

Brook, G.A., Kirkbride, M.P., Brock, B.W. (2006). "Cirque development in a steadily uplifting range: rates of erosion and long-term morphometric change in alpine cirques in the Ben Ohau Range, New Zealand." Earth Surface Processes and Landforms 31(9): 1167-1175.

Clark, D.H. and Gillespie, A.R. (1996). "Timing and significance of Late-glacial and Holocene cirque glaciation in the Sierra Nevada, California." Quaternary International 38-39: 21-38

Cohen, D., Hooyer, T.S., Iverson, N.R. (2006). "Role of transient water pressure in quarrying: A subglacial experiment using acoustic emissions." Journal of Geophysical Research –Earth Surface 111(F3) F03006

Evans, I.S. and Cox, N.J. (1995). "The form of glacial cirques in the English Lake District, Cumbria." Zeitschrift fuer Geomorphologie 39(2): 175-202

Garcia-Ruiz, J.M., Gomez-Villar, A., Ortigosa, L., Marti-Bono, C., (2000). "Morphometry of glacial cirques in the central Spanish Pyrenees." Geografiska Annaler. Series A: Physical Geography 82(4): 433-442

Gillespie and Zehfuss (2004). "Glaciations of the Sierra Nevada, California, USA." Quaternary Glaciations –Extent and Chronology Part II. Elsevier B.V.

Goldsby, D. L., and D. L. Kohlstedt (2001). "Superplastic deformation of ice: Experimental observations." Journal of Geophysical Research, 106(B6), 11,017–11,030.

Gordon, J.E. (1977). "Morphometry of cirques in the Kintail-Affric-Cannich area of Northwest Scotland." Geografiska Annaler. Series A: Physical Geography 59(3-4): 177-194

Gordon, J.E. (2001). "The corries of the Cairngorm Mountains." Scottish Geographical Journal 117(1): 49-62

Hallet, B. (1979). "A theoretical model of glacial abrasion." Journal of Glaciology 23(89): 39-50.

Hallet, B. (1996). "Glacial quarrying: a simple theoretical model." Annals of Glacialogy 22: 1-8.

Hallet, B., L. et al. (1996). "Rates of erosion and sediment evacuation by glaciers: a review of field data and their implications." Global Planetary Change 12: 213-235.

Harbor, J.M., Hallet, B., Raymond, C.F., (1988). "A numerical model of landform development by glacial erosion." Nature 333: 347-349.

Harbor, J.M., Sharp, M., Copland, L., Hubbard, B. (1997). "Influence of subglacial drainage conditions on the velocity distribution within a glacier cross section." Geology (Boulder) 25(8): 739-742

Harbor, J. M. (1992). "Numerical modeling of the development of U-shaped valleys by glacial erosion." Geological Society of America Bulletin 104: 1364-1375.

Harbor, J.M. (1995). "Development of glacial-valley cross sections under conditions of spatially variable resistance to erosion." Geomorphology 14(2): 99-107

Haynes, V.M. (1998) "The morphological development of alpine valley heads in the Antarctic Peninsula." Earth Surface Processes and Landforms 23: 53-67

Hooke, R. L. (1991). "Positive feedbacks associated with erosion of glacial cirques and overdeepenings." Geological Society of America Bulletin 103: 1104-1108.

Hooke, R.L., Calla, P., Holmlund, P., Nilsson, M., Stroeven, A., (1989). "A 3 year record of seasonal variations in surface velocity, Storglaciaren, Sweden." Journal of Glaciology 35: 235-247.

Hooke, R. L. and Pohjola, V. A. (1994). "Hydrology of a segment of a glacier situated in an overdeepening, Storglaciären, Sweden." Journal of Glaciology 40(134): 140-148.

Humphrey, N. F. and C. F. Raymond (1994). "Hydrology, erosion, and sediment production in a surging glacier: Variegated Glacier, Alaska, 1982-83." Journal of Glaciology 40(136): 539-552.

Iken, A. (1981). "The effect of the subglacial water pressure on the sliding velocity of a glacier in an idealized numerical model." Journal of Glaciology 27(97): 407-421.

Iverson, N.R. (1990). "Laboratory simulations of glacial abrasion: comparison with theory." Journal of Glaciology (36): 27-36.

Iverson, N. R. (1991). "Potential effects of subglacial water-pressure fluctuations on quarrying." Journal of Glaciology 37(125): 27-36.

Iverson, N. R. (1993). "Regelation of ice through debris at glacier beds: Implications for sediment transport." Geology 21: 559-562.

Janssen, K.N., Kleman, J., Marchant, D.R. (2002). "The succession of ice-flow patterns in north-central Quebec-Labrador, Canada." Quaternary Science Reviews 21(4-6): 503-523.

Johnson, (1904). "The profile of maturity in Alpine glacial erosion." Journal of Geology: 569-578

Kessler, M. A. and Anderson, R. S. (2004). "Testing a numerical glacial hydrological model using spring speed-up events and outburst floods." Geophysical Research Letters 31: doi:10.1029/2004GL020622.

Kleman, J. (1990). "On the use of glacial striae for reconstruction of paleo-ice sheet flow patterns." Geografiska Annaler. Series A Physical Geography 72(3-4): 217-236

MacGregor, K. C., Anderson, R.S., Waddington, E.D. (2000). "Numerical simulations of glacial valley longitudinal profile evolution." Geology 28: 1031-1034.

MacGregor, K.C., Anderson, R.S., Waddington, E.D. (2009). "Numerical modeling of glacial erosion and headwall processes in alpine valleys." Geomorphology 103(2): 189-204.

Marshall, H.P., Harper, J.T., Pfeffer, W.T., Humphrey, N.F. (2002). "Depth varying constitutive properties observed in an isothermal glacier." Geophysical Research Letters 29(23): 4

Matthes, F.E. (1900). "Glacial sculpture of the Bighorn Mountains, Wyoming." Science 11: 507

Matthews, R.A. and Burnett, J.L. (1965). Geologic Map of California, Fresno sheet: California Division of Mines an Geology

McCall, J.G., (1972). "The flow characteristics of a cirque glacier and their effect on cirque formation." In: Embleton, C. (Ed), Glaciers and Glacial Erosion. Macmillan Press, New York, pp. 205-228

Molnar, P. and P. England (1990). "Late Cenozoic uplift of mountain ranges: chicken or egg?" Nature 346: 29-34.

Montgomery, D. R. (2002). "Valley formation by fluvial and glacial erosion." Geology 30(11): 1047-1050.

Naylor, S. and Gabet, E.J. (2007). "Valley asymmetry and glacial versus nonglacial erosion in the Bitterroot Range, Montana, USA." Geology 35(4): 375-378.

Oerlemans, J., (1984). "Numerical experiments on large-scale glacial erosion." Zeitschrift fur Gletscherkunde und Glazialgeologie 20: 107-126

Olyphant, Greg A. (1981). "Allometry of cirque evolution." Geological Society of America Bulletin 92: 679-685.

Oskin, M. E. and Burbank, D. W. (2005). "Alpine landscape evolution dominated by cirque retreat." Geology 33(12): 933-936.

Paterson, W.S.B. (1994). "The Physics of Glaciers." Pergamon/Elsevier Science Ltd., Tarrytown, NY

Peterson, P.F. (1992). "A method for predicting and minimizing numerical diffusion." Numerical Heat Transfer 21: 343-366

Rapp, A., (1984). "Nivation hollows and glacial cirques in Soderasen, Scania, South Sweden." Geografiska Annaler 42A: 71-200

Raymo, M. E. and Ruddiman,W. F. (1992). "Tectonic forcing of late Cenozoic climate." Nature 359: 117-122.

Rothlisberger, H. (1972). "Water pressure in intra- and sub-glacial channels." Journal of Glaciology 11: 177-203.

Sugden, D.E. (1969). "The age and form of cories in the Cairngorms." Scottish Geographical Magazine 85: 34-46

Trenhaile, A.S. (1974). "Cirque elevation in the Canadian Cordillera." Annals of the Association of American Geographers 65(4): 517-529